



Full length article

# Development and evaluation of rapid, national-scale outdoor air pollution modelling and exposure assessment: Hybrid Air Dispersion Exposure System (HADES)

Calvin Jephcote<sup>a,\*</sup> , John Gulliver<sup>b</sup> <sup>a</sup> Centre for Environmental Health and Sustainability, University of Leicester, United Kingdom<sup>b</sup> Population Health Research Institute, City St George's, University of London, United Kingdom

## ARTICLE INFO

## Keywords:

Air pollution  
Dispersion modelling  
Exposure assessment  
Nitrogen dioxide  
Ozone  
Regression calibration

## ABSTRACT

Improvements in computer processing power are facilitating the development of more detailed environmental models with greater geographical coverage. We developed a national-scale model of outdoor air pollution (Hybrid Air Dispersion Exposure System – HADES) for rapid production of concentration maps of nitrogen dioxide (NO<sub>2</sub>) and ozone (O<sub>3</sub>) at very high spatial resolution (10m). The model combines dispersion modelling with satellite-derived estimates of background concentrations, land cover, and a 3-D representation of buildings, in a statistical calibration framework. We developed an emissions inventory covering England and Wales to implement the model and tested its performance using concentration data for the years 2018–2019 from fixed-site monitoring locations. In 10,000 Monte Carlo cross-validation iterations, hourly-annual average R<sup>2</sup> values for NO<sub>2</sub> were 0.77–0.79 (RMSE: root mean squared error of 5.3–5.7 µg/m<sup>3</sup>), and 0.87–0.89 for O<sub>3</sub> (RMSE = 3.6–3.8 µg/m<sup>3</sup>) at the 95% confidence interval. The annual average R<sup>2</sup> was 0.80 for NO<sub>2</sub> (RMSE = 4.9 µg/m<sup>3</sup>) and 0.86 for O<sub>3</sub> (RMSE = 3.2 µg/m<sup>3</sup>) from aggregating the hourly-annual estimates. The air pollution surfaces are freely available for non-commercial use. In using these surfaces for exposure assessment, all residential locations, and neighbourhoods in urban areas, are unlikely to be below the 2021 World Health Organisation Air Quality Guidelines threshold (10 µg/m<sup>3</sup>) for annual average NO<sub>2</sub> concentrations (10 µg/m<sup>3</sup>). Rural and suburban areas are likely to exceed the peak-season 8-hour daily maximum O<sub>3</sub> threshold (60 µg/m<sup>3</sup>).

## 1. Introduction

There is strong evidence published over decades linking outdoor air pollution to harmful effects on human health (Brunekreef and Holgate, 2002; Dominici et al., 2021). In recent years, the gradual cessation of fossil fuel combustion, the uptake of alternative cleaner fuels, and improvements in emissions technologies from a range of sources (i.e., motorised vehicles and industry), has resulted in lower levels of air pollution, especially in developed countries, with poorer air quality remaining in other parts of the world. Notwithstanding improvements to air quality in many areas, harmful effects on health have been shown to persist at relatively low levels of air pollution including gases and particles (Dominici et al., 2019; Brunekreef et al., 2021; Brauer et al., 2022). The World Health Organisation (WHO) revised their guidelines on limit values for air pollution in 2021 to reflect the need to safeguard human health at lower levels of air pollution than previously recognised as safe

(WHO, 2021). The recommended annual average concentration for nitrogen dioxide, for example, was reduced from 40 µg/m<sup>3</sup> in 2005 to 10 µg/m<sup>3</sup>.

To inform regulation and guidelines, air pollution monitoring has increased globally, but the density of sites does not capture the variability in population exposures in many locations. Instead, methods have been developed to produce maps of air pollution, especially for exposure assessment. Most national-scale modelling at high spatial resolution (< 100m) has used the principles of land use regression (LUR) due to the computational barriers of running dispersion models. LUR (Hoek et al., 2008) uses surrogates to represent air pollution sources (e.g., distance from road, traffic intensity within a zone) and sinks (e.g., green space) calibrated to measurements of air pollution. LUR is a conceptually simple and efficient technique for detailed mapping over large geographical areas. The main inherent weakness of LUR and related statistical techniques (e.g., machine learning and geostatistical

\* Corresponding author at: School of Geography, Geology and the Environment, University of Leicester, LE1 7RH, UK.

E-mail address: [cj191@leicester.ac.uk](mailto:cj191@leicester.ac.uk) (C. Jephcote).

<https://doi.org/10.1016/j.envint.2025.109304>

Received 7 October 2024; Received in revised form 13 January 2025; Accepted 23 January 2025

Available online 25 January 2025

0160-4120/© 2025 The Authors. Published by Elsevier Ltd. This is an open access article under the CC BY license (<http://creativecommons.org/licenses/by/4.0/>).

methods), however, is in not reflecting well the effects of meteorology and atmospheric processes on patterns of air pollution, and not dealing well with discrete sources of lower density such as industrial area and point sources. Ideally, detailed air pollution maps would use deterministic methods (i.e., dispersion modelling), reflecting environmental and atmospheric processes. As computational barriers are now being overcome more easily, examples of fine-scale, dispersion modelling, or hybrid air pollution models (e.g., dispersion modelling, LUR, and satellite data), have been developed in recent years, but tend to be limited

to single cities (Korek et al., 2017; Tularam et al., 1987; Dimakopoulou et al., 2022; Kilbo Edlund et al., 2024; Masey et al., 2018). There are very few examples of high resolution, national-scale dispersion models (Klompaker et al., 2021).

For the United Kingdom (UK) and its nations, the only national-scale, open data for outdoor regulatory air pollutants was ‘background concentration mapping’ available from the UK Government Department for Environment Food and Rural Affairs (Defra) at <https://uk-air.defra.gov.uk/data/gis-mapping>. The mapping to a 1km x 1km grid does not,

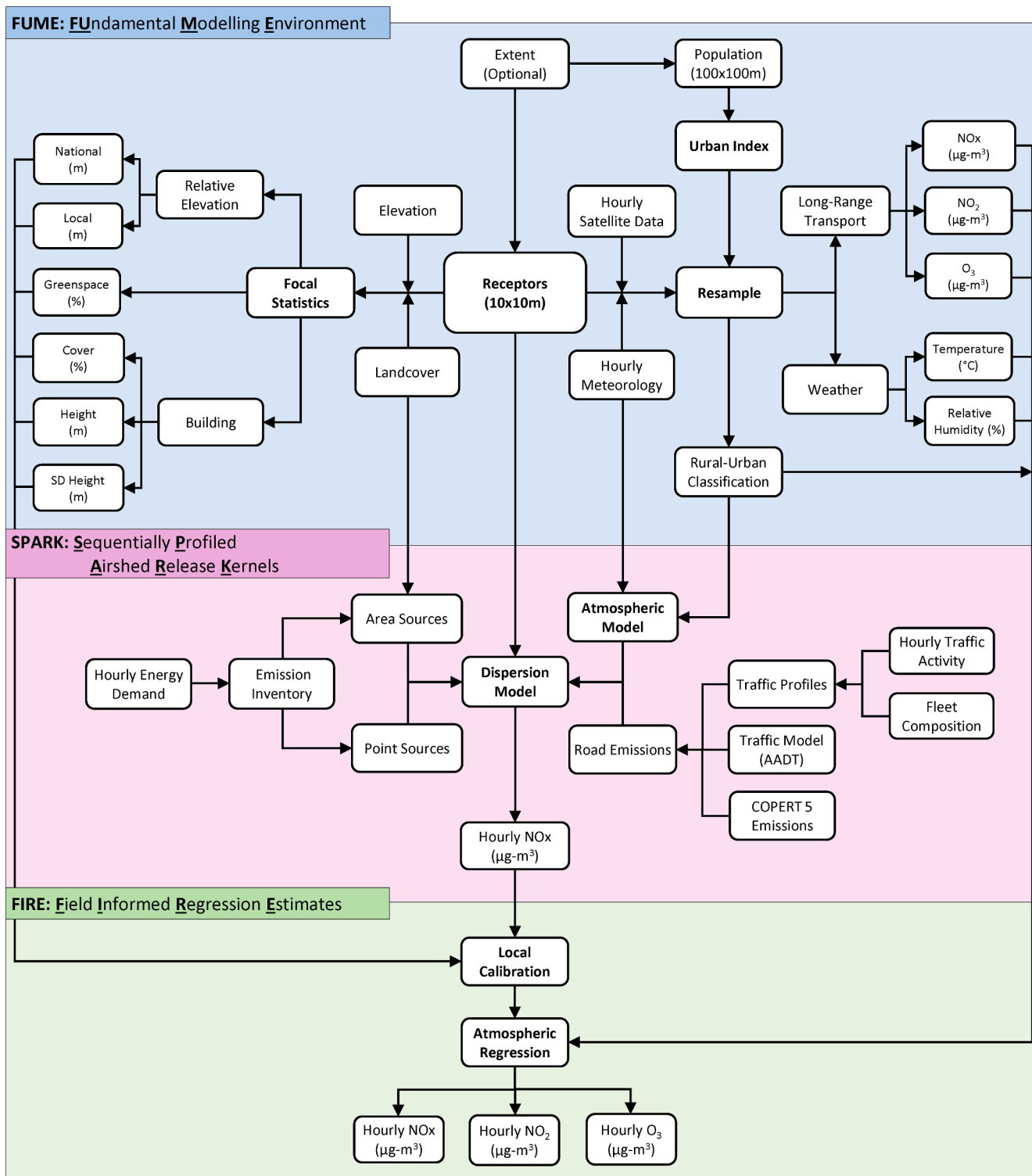


Fig. 1. HADES modelling procedure.

however, provide the basis for representing local (intra-urban variability) air pollution patterns, nor does it provide a useful basis for exposure assessment. There have been some higher resolution data produced from statistical approaches for specific time points based on LUR for Great Britain (Gulliver et al., 2013, Wang et al., 2022) and for the UK as part of models for Europe (de Hoogh et al., 2018), however, these datasets are not readily available. To address the limitation of existing approaches and outputs, we developed a ‘Hybrid Air Dispersion Exposure System’ (HADES) modelling framework to produce high spatial resolution, national air pollution maps. HADES uses Gaussian plume dispersion modelling to quantify the local and regional atmospheric fate of emissions from individual air pollution sources (e.g., roads, housing, and industry), satellite derived long-range chemical transport models (CTMs), and other surrogates of dispersion, retention, and removal based on landform and use within a statistical calibration framework. For the test application, the aim was to evaluate model performance against data from a network of fixed-site monitors, and then produce high resolution (10m), annual and hourly-annual air pollution maps, covering England and Wales, for the main regulatory outdoor gaseous air pollutants: oxides of nitrogen (NO<sub>x</sub>), nitrogen dioxide (NO<sub>2</sub>) and ozone (O<sub>3</sub>). HADES was developed to allow the use of open-access input data with near-global coverage.

## 2. Methods

HADES comprises of a meteorological pre-processor, road-transport emission model, emission inventory resampling, source-specific GIS-based air pollution dispersion models, and topographic-atmospheric concentration correction procedures via regression modelling. Fig. 1 shows the overall structure and data flow protocols within HADES via three, main modules: (1) FUME – Fundamental Modelling Environment, (2) SPARK – Sequentially Profiled Airshed Release Kernels, and (3) FIRE – Field Informed Regression Estimates. In FUME, topographic and atmospheric data are integrated into the model and prepared for the source specific dispersion modelling of NO<sub>x</sub> (SPARK). The downstream regression analysis combines output from SPARK with local geometry, climatic, and long-range air pollution influences to calculate the total concentration of NO<sub>x</sub>, NO<sub>2</sub>, and O<sub>3</sub> (FIRE). Appendix 1 provides an overview of the data used in model development and calibration, complementing the model flow established in Fig. 1.

FIRE, runs two local geometry calibration models on the NO<sub>x</sub> dispersion surfaces (C1 and C2), which are followed by three models to determine the cyclic photochemical conversion of NO<sub>x</sub> to NO<sub>2</sub> and O<sub>3</sub> (M1, M2, and M3). C1 calibrates the road-transport NO<sub>x</sub> dispersion component to account for kerbside, street canyon, and relative elevation influences. C2 calibrates the ‘Area’ and industrial ‘Point’ source NO<sub>x</sub> dispersion components using ventilation and surface deposition parameters (i.e., building density, local and regional elevation). M1 combines C1 and C2 to calculate total NO<sub>x</sub> concentrations. M2 and M3 account for the photochemical conversion to NO<sub>2</sub> and O<sub>3</sub> based on local and long-range CTM contributions, photochemical reactions, and pollutant sinks. The regression parameters found in HADES are constructed from air pollution measurements in the automatic monitoring network of the UK.

HADES accounts for local (i.e., 10m x 10m road-transport emissions within 500m), regional (i.e., 1km x 1km area source emissions and industrial point sources within 4km), and long-range (i.e., 10km x 10km satellite derived CTM) contributions to the photochemical nitrogen cycle, from data with varying spatial resolutions that reflect the rate of divergence from source. Pollution surfaces are modelled at a 10m resolution.

### 2.1. Data requirements

#### 2.1.1. Topography

Topographic information can be obtained from a variety of open

access sources. However, datasets compiled by national mapping agencies are preferable for reasons of spatiotemporal accuracy and precision.

In this case we used data from the Ordnance Survey MasterMap (OSMM) product as it has complete coverage of the permanent spatial features in Great Britain (GB). OSMM is updated quarterly using ground and aerial survey, with an absolute positional accuracy of 0.9m, 2.4m, and 8.8m in urban, rural, and remote rural areas at the 99% confidence level, respectively (OS, 2023). The relative positional accuracy (to other local polygon features) in urban and rural areas is  $\pm 1.1\text{m}$  (0–60m) and  $\pm 2.5\text{m}$  (0–100m), respectively at the 99% confidence level. The dataset contains height attributes modelled from synthetic-aperture radar for 95% of the buildings in Great Britain, with vertical measurement errors  $< 0.1\text{m}$ . Thematic records were reclassified to eleven classes reflective of landcover in regions with a temperate climate: ‘Agricultural Land’, ‘Air Traffic’, ‘Commercial Buildings’, ‘Grassland’, ‘Industrial Buildings’, ‘Industrial Land’, ‘Railways’, ‘Residential Buildings’, ‘Trees’, ‘Waterways’, and ‘Wetland’. This simplification ensures reproducibility with other data, whilst maintaining sufficient detail to map against CORINAIR SNAP sector emissions by land use (EEA, 1996).

OSMM spatial polygon features were converted to two 10m raster surfaces – these are simply matrices with georeferenced gridded values separated by a uniform distance. The first surface records primary land use, as defined by the majority area coverage within each cell. The second surface records building height, based on the area-weighted average of intersected building footprints. Appendix 2 thematically summarises the OSMM building height profiles, to assist model runs in locations where such information is not readily available. A Digital Elevation Model (DEM) representation the height of the earth’s surface above sea level is also required. The European Environment Agency (EEA) EU-DEM version 1.1 Pan-European raster surface recording elevation at a 25m resolution was used in this analysis.

Open access topographic information for many countries can be accessed from OpenStreetMap and thematically improved by Wikimapia, with varying levels of accuracy and completeness. Across Europe, CORINE surfaces can be used to define land cover at a 100m resolution, with the Urban Atlas providing partial coverage of building heights at a 10m resolution for 2012. Google with their ‘Open Buildings 2.5D Temporal Dataset’, and Microsoft are also using machine learning to develop open access building footprint and height datasets with global coverage.

#### 2.1.2. Emissions inventories

The UK Government annually compiles a National Atmospheric Emission Inventory (NAEI) for regulatory compliance with the European Monitoring and Evaluation Programme (EMEP) and United Nations Framework Convention on Climate Change (UNFCCC). The UK NAEI collects ‘Point’ source emission records (from large industrial stacks), and models releases that are too small and numerous to be inventoried at a 1km x1km resolution (known as ‘Area’ sources) by CORINAIR SNAP sector. ‘Area’ source emissions for individual SNAP sectors were resampled to 10m raster surfaces, by equally allocating the releases in a 1km tile to relevant land use cells nested within. ‘Point’ source emissions were summated on a 10m raster surface. Appendix 3 summarises the distribution of ‘Area’ source emission releases (g/s) across England and Wales in 2019, to assist model runs in locations with limited information.

Road-transport emissions (SNAP sector 7) were not extracted from the NAEI database. It is preferable to model these as individual ‘Line’ sources using spatiotemporally detailed local information. Annual average daily traffic (AADT) flows in 2013 were modelled on all major and minor roads in GB (Morley and Gulliver 2016). This simulated road network approach can be replicated in other locations using OpenStreetMap and traffic counts on major roads. AADT values were locally scaled in accordance to spatiotemporal changes at 36,626 traffic count sites across GB, creating annual traffic estimates for 2010–2020 (see Appendices 4-5).

Section 2.2.2 outlines the procedure to disaggregate modelled traffic flows by vehicle class, and apply speed-emission equations to produce NOx emission rates (g/s per meter) for each road link. The road transport emission rates were then multiplied by road length and aggregated to a 10m raster surface.

Annual-average emission releases from 'Area', 'Point', and 'Line' sources were scaled to hourly release estimates using relevant activity profiles. 'Area' and 'Point' sources are assumed to be largely derived from anthropogenic sources, and they were therefore linked to hourly average energy demands in the national electricity grid (Appendix 6). A distribution profile of total traffic counts by time-of-day, informed the hourly release estimates on roads (Appendix 7).

### 2.1.3. Weather

Weather observations were obtained from the open access National Oceanic and Atmospheric Administration Integrated Surface Database (ISD) via <https://www.ncei.noaa.gov/data/global-hourly> (NOAA, 2018). The ISD currently contains hourly records at >14,000 active surface meteorological sites from around the world, and historic data (since 1901 in some instances) is available at >35,000 sites. ISD integrates data from >100 sources, using algorithms to provide records in a consistent format, correcting for random and systematic errors (Lott 2003).

HADES requires hourly measurements of wind speed and direction, dry air temperature, and dew point. Records of atmospheric pressure, cloud cover, and the cloud base height can improve the definition of atmospheric conditions, when available. Stineman (1980) interpolation was used to update missing weather records, where less than six previous or subsequent hours of the time-series were missing. This method is statistically more accurate than cubic splines, minimising overshoot and inflection errors (Perillo and Piccolo 1991).

For context, there were 188–191 active stations across Great Britain in 2018–2020, of which 96% collected hourly wind and temperature data for ≥75% of the year. Hourly atmospheric pressure and cloud data was recorded at 62.8–64.4% of these stations for ≥75% of the year. On average, the minimum distance from one weather station to another is 23.9km (SD = 15.7km).

Relative humidity (RH) is calculated from the temperature records. Firstly, vapour pressure ( $e$ ) is estimated in Pascals using an enhanced Magnus-Tetens formula with a <0.4% relative error (Alduchov and Eskridge 1996):

$$e = \begin{cases} 610.94 * \exp\left(\frac{T * 17.625}{T + 243.04}\right) & \text{where } T \geq 0 \\ 611.21 * \exp\left(\frac{T * 22.587}{T + 273.86}\right) & \text{where } T < 0 \end{cases} \quad (1a)$$

Where  $T$  is the dry air temperature measured in degree Celsius. Equation (1a) is then repurposed to calculate the saturated vapour pressure ( $e_s$ ), by using the dew point temperature ( $T_d$ ) recorded by the measurement station instead of  $T$ . Finally, RH is determined by:

$$RH(\%) = 100 * \left(\frac{e}{e_s}\right) \quad (1b)$$

RH measures the amount of water vapour present in air, expressed as a percentage of the amount needed for saturation at the current air temperature. When RH reaches 100%, the air is totally saturated, increasing the likelihood of rain and the wet deposition of nitrogen. The removal of gaseous air pollutants by vegetation is also increased under high RH levels.

### 2.1.4. Remote sensing

Satellite informed long-range chemical transport model data was accessed from the Copernicus Atmosphere Monitoring Service (CAMS) at <https://ads.atmosphere.copernicus.eu>. The 'CAMS European air

quality reanalyses' dataset provides hourly surface level model estimates of nitrogen dioxide and ozone at a 0.1° resolution (approximately 10km x 10km). CAMS observations are used to account for the long-range transportation of air pollutants, and its (regional and international) influence on background concentrations by time of day. This open access dataset has pan-European coverage, temporally backdated to 2013.

For other applications, CAMS global pollutant observations can be accessed at 3-hour intervals at a 0.1° resolution (approximately 80km x 80km) via its 'ECMWF Atmospheric Composition Reanalysis 4' product. There is the potential to improve the spatial resolution of these records, if harmonised with alternative satellite products. For instance, NO<sub>2</sub> can be estimated from MODIS 8-day average surface reflectance values at a 1km resolution (Zhou et al 2010).

### 2.1.5. Demography

Annual global population count raster surfaces at a 100m resolution for 2000–2020, are available through the WorldPop open repository <https://www.worldpop.org>. WorldPop gridded datasets are created with machine learning dasymetric mapping techniques to resample census and survey records to residential related land uses described by local vector data, aerial, and satellite imagery (Stevens et al 2015).

We have devised a hybrid classification scheme called the Urban Index, which is based on established European Commission (EC, 2014) and OECD (OECD, 2016) urban–rural population density thresholds (Appendix 1). This scheme considers population counts in local and adjacent cells of the gridded surface to create a 0–1 index that records urban centres with a value of 1.

## 2.2. Model development

### 2.2.1. Data Preparation

Several of the collected datasets may need to be resampled to a common spatial resolution, based on the Inverse-Distance Weighting (IDW) of nearby observations (Fig. 1; FUME). This linear interpolation technique is fast, and preferred if there are large volumes of densely sampled and evenly distributed spatial data to process.

HADES model parameters are created with the subsequent dispersion models, or by spatial statistics that reflect influences within the nearby vicinity of a given location. The final set of land use parameters capture the urban canyon effect (i.e., surface roughness, building-downwash, and containment effects), the effects of elevation contrast (i.e., atmospheric flow and plume deposition), weather influences on photochemical oxidants, vegetation sinks, and long-range transportation processes. Appendix 1 describes how the model parameters are created, their upper and lower limits (reflective of the training data), and the required transformation procedures to account for nonlinear relationships. The following equation is used to conduct neglog transformations (Whittaker et al 2005, p.866):

$$\text{neglog}(x) = \begin{cases} -1 * \log((-1 * x) + 1) & \text{where } x \leq 0 \\ \log(x + 1) & \text{where } x > 0 \end{cases} \quad (2)$$

### 2.2.2. Traffic emissions model

UK Department for Transport (DfT) vehicle statistic tables were accessed via <https://www.gov.uk/government/collections/vehicles-statistics>. Cross-tabulations were used to split the modelled AADT counts into five vehicle categories by road class and geography: Cars, Buses, Heavy Goods Vehicles (HGVs), Light Goods Vehicles (LGVs) used by commercial transport, and Motorcycles. Geographic variations in fleet profiles were then accounted for across 205 local authority counties and by urban–rural status in GB.

UK DfT records of vehicle ownership by category, specific model, and year of manufacture were used to create annual fleet profiles based on fuel type, emission standard, engine capacity, and age. These profiles considered the vehicle attributes of 45.0 thousand car, 11.1 thousand

LGV, 9.1 thousand motorcycle, 1.5 thousand HGV, and 0.3 thousand unique models of buses operating on UK roads between 2010 and 2020. For additional context, there were 32.9 million cars (84.1%), 4.4 million LGVs (11.2%), 1.2 million motorcycles (3.2%), 0.5 million HGVs (1.4%), and 0.1 million buses (<0.1%) licensed across the UK in 2019. These national fleet profiles were used to further disaggregate the spatially resolved AADT counts into 206 vehicle categories. Fleet profiles were updated when a road links falls within a low emission zone, to ensure full compliance with local restrictions.

Vehicle speeds were initially defined by UK national speed limits of 30mph for restricted access (residential and unclassified), 60mph for single-carriageway (tertiary, secondary, and primary roads), and 70mph for motorways and trunk roads. Heavy vehicles are restricted to 50mph on single carriageways, and 60mph on motorways and trunk roads. Road link speeds were set to half the limit for general vehicles. Road speeds were then restricted in populated urban locations, using a scaling factor created by multiplying the Urban Index fraction by 0.33 (i.e., a maximum soft speed limit reduction of 33% in urban locations creates a 20mph zone).

EU standard road vehicle emission factors for NO<sub>x</sub> were obtained from COPERT v5.0 speed-emission equations (BEIS, 2017). Emission functions were allowed to differ by road incline (-6% to +6%) for the 63 different HGV categories. The interquartile range of NO<sub>x</sub> emission from the HGV fleet increases by 34-117% on high incline roads (with bidirectional traffic). Scaling factors were then applied to account for fuel purity, and emission degradation due to vehicle age and projections of accumulated mileage in the UK fleet (DfT, 2009). Electric vehicles are without a combustion source, and therefore have zero tailpipe emissions when modelling oxides of nitrogen.

A workbook containing the resulting UK vehicle fleet profiles and emission formulas is provided as supplementary materials, to assist with HADES applications in locations with sparse vehicle records (see the 'HADES traffic toolkit'). Alternatively, Appendix 8 summarises the distribution of emission releases as 'grams per second per meter of road length', across England and Wales in 2019 by road class.

The road transport emission rates were then multiplied by road length, intersected with, and aggregated to a 10m raster surface. HADES treats road-transport as a series of point releases along the road network. Annual-average emission rates were scaled to hourly-annual average releases using a distribution profile of hourly total traffic counts on all road types in Great Britain, for a typical weekday in the specified year (Appendix 7).

### 2.2.3. Meteorological pre-processor

The direction and magnitude of plume dispersion in HADES is informed by hourly estimates of atmospheric stability, and measurements of wind speed and direction. Atmospheric stability measures the tendency for an air parcel to rise or resist vertical motion, as it is horizontally displaced by the prevailing wind. These three processes are the main determinants of how pollutants released into the lower atmosphere are dispersed.

The United States Environmental Protection Agency (USEPA, 2000) recommends that regulatory air quality modelling applications use Pasquill (1961) stability categories with Turner's (1964) revised method for routinely collected surface station weather data. Pasquill-Turner categories cover highly turbulent (A), neutral (D), and extremely stable day (F) or night-time (G) conditions.

Firstly, the solar elevation angle ( $\Psi$ ), or the angle of the sun above the local horizon, is calculated in degrees via (Stull 1988, p.257–258):

$$\delta = 0.49 * \cos\left(\frac{2\pi * (d - 173)}{365.25}\right) \quad (3a)$$

$$h = \pi * \left(\frac{t_{UTC}}{12}\right) - \lambda \quad (3b)$$

$$\Psi = \sin^{-1}(\sin\phi * \sin\delta - \cos\phi * \cos\delta * \cosh) * \frac{180}{\pi} \quad (3c)$$

Where,  $\delta$  records the angle of the sun above the equator in radians (the solar declination angle),  $d$  is the Julian day number (1 to 366),  $h$  is the solar hour angle in radians,  $t_{UTC}$  is the coordinated universal time, with  $\phi$  and  $\lambda$  recording latitude (positive north) and longitude (positive east) in radians. The solar elevation angles are then converted to solar insolation codes, where  $0^\circ = 0$  (none),  $1-15^\circ = 1$  (weak),  $16-35^\circ = 2$  (slight),  $36-60^\circ = 3$  (moderate), and  $>60^\circ = 4$  (strong) (USEPA 2000, p.61).

The Pasquill-Turner scheme also requires hourly measurements of the following sky conditions: wind speed (m/s), cloud base height (ft above ground level), and estimates of how many eighths of the sky are covered in cloud (0 Oktas = clear, 8 Oktas = overcast). Appendix 9 describes how these four components are consolidated into Pasquill-Turner categories.

Within the UK, approximately a third of all weather stations fail to regularly collect all components of the Pasquill-Turner scheme (i.e., missing instruments or through measurement and record errors). Therefore, HADES calculates a second stability scheme that only requires measurements of wind speed and direction. The United States Nuclear Regulatory Commission (USNRC, 1972) has historically measured standard deviations in horizontal wind fluctuations (Sigma-Theta) to approximate stability, where small deviations are associated with stable conditions. This approach was later adapted to account for wind speeds, known as the Modified-Sigma-Theta (MST) approximation of atmospheric stability (Mitchell 1982).

Standard deviations in wind direction ( $\sigma_\theta$ ) are calculated according to Yamartino (1984, p.1363–5):

$$\epsilon = \sqrt{1 - \left( \left( \frac{1}{n} * \sum_{i=1}^n \sin\left(\theta_i * \left(\frac{\pi}{180}\right)\right) \right)^2 + \left( \frac{1}{n} * \sum_{i=1}^n \cos\left(\theta_i * \left(\frac{\pi}{180}\right)\right) \right)^2 \right)} \quad (4a)$$

$$\sigma_\theta = \sin^{-1}(\epsilon) * \left(1 + 0.1547 * \epsilon^3\right) * \left(\frac{180}{\pi}\right) \quad (4b)$$

Where  $\theta_i$  represents the wind angle for observation  $i$ , and  $n$  is the total number of observations considered.  $\epsilon$  accounts for the east–west and north–south components of wind.

Sigma-Theta is typically calculated from measurements at 10-minute intervals over a 1-hour averaging time (Mitchell 1982). HADES employs an experimental MST approach for hourly surface measurements, whereby a moving time window of  $\pm 2$  hours is centred on the hour of interest (i.e., SD of five hourly observations). Sigma-Theta, measured wind speed, and the solar angle (see equations 3a-3c) determining if it is day or night for the hour of interest, are then checked against the MST stability table to return an approximate Pasquill stability category (Appendix 10).

HADES computes an arithmetic average of the Pasquill-Turner (where available) and the MST stability schemes for dispersion modelling. The two schemes appear to adequately capture diurnal changes in stability and their profiles have reasonable agreement, which typically deviate by a single class (Appendix 11). MST corrects the Pasquill-Turner classifications tendency to favour neutral conditions, and the Pasquill-Turner scheme reduces the frequency of extreme stability conditions recorded by MST. The use of the MST stability scheme increases the spatial resolution of weather influences, and allows for model applications in locations with sparse data.

### 2.2.4. Dispersion modelling

HADES uses gaussian dispersion plume models to quantify the atmospheric fate of individual air pollution sources at ground level (Turner 1970, p5):

$$C(x, y, z) = \left( \frac{Q}{2\pi\sigma_y\sigma_zU} \right) * \exp \left[ -0.5 * \frac{y^2}{\sigma_y^2} \right] * \left( \exp \left[ -0.5 * \frac{(z-H)^2}{\sigma_z^2} \right] + \exp \left[ -0.5 * \frac{(z+H)^2}{\sigma_z^2} \right] \right) \quad (5)$$

Where  $C$  is the pollutant concentration at a receptor location that has a height of  $z$  meters above ground level (set at 1m to reflect air entering the human respiratory system), at a measured distance in meters downwind of the pollutant source on the  $x$  and  $y$  axis. The  $x$ -axis is the centreline direction of the plume, and the  $y$ -axis is lateral to wind direction.  $Q$  is the emission source rate (g/s),  $U$  is the wind speed (m/s), and  $H$  is the effective height of the plume above ground at source (m).

The effective plume height ( $H$ ) is a summation of the stack height ( $H_s$ ) and the initial plume rise ( $H_r$ ), which is calculated using (Carson & Moses 1969, p866):

$$H = H_s + H_r \quad (6a)$$

$$H_r = \lambda * \left[ \left( -0.029 * \left( \frac{V * D}{U} \right) \right) + \left( 5.35 * \frac{Q_h^2}{U} \right) \right] \quad (6b)$$

Where  $V$  is the stack gas exit velocity (meters per second),  $D$  is the stack exit diameter (m),  $U$  is the wind speed at stack exit (m/s),  $Q_h$  is the heat emission rate (KJ/s), and  $\lambda$  is a stability correction factor. The following function was fitted to extend Carson & Moses (1969) stability correction factors across the Pasquill stability categories ( $P_s$ ), which are converted from alphabet letters to descending numbers (i.e., A = 1, D = 4 and G = 7):

$$\lambda = 2.6845 * (P_s^{-0.689}) \quad (6c)$$

The parameters required to calculate plume rise are source specific. Parameters for cars were used to derive road-transport plume heights, where a tailpipe height ( $H_s$ ) of 0.2m and exhaust diameter ( $D$ ) of 0.06m is typical. We approximate  $Q_h$  as 12.96 KJ/s for cars operating across gears 3–6 in environments of 1013mb and 15°C, where  $V$  equals 15 m/s (Madaro et al 2020).  $H$  was set to a minimum height of 1.5 m to reflect traffic-induced turbulence. Based on these parameters, road-transport effective plume heights of 24.4, 10.1, and 6.4m are expected for wind speeds of 2 m/s at stability classes A, D, and G, respectively (Appendix 12).

UK and European emission inventories tend to only record pollutant emission rates, with other stack parameters not routinely collected or made freely available. Representative plume rise profiles for ‘Area’ and ‘Point’ sources were derived from the US state of Pennsylvania’s emissions inventory, which contained detailed records for 7,332 vertical stacks in 2019 (Appendix 13). The subsequent parameters used for ‘Area’ sources are:  $H_s = 5m$ ,  $D = 0.6m$ ,  $V = 13.64$  m/s, and  $Q_h = 225.19$  KJ/s. For ‘Point’ sources:  $H_s = 10m$ ,  $d = 0.6m$ ,  $V = 13.21$  m/s, and  $Q_h = 413.64$  KJ/s. Based on these parameters, effective plume heights can range from 32.2–111.1m and 46.9–153.9m at wind speeds of 2 m/s for ‘Area’ and large industrial ‘Point’ sources, respectively. Regulatory pollutant models typically use a default effective plume height of 10m for all sources to reflect typical stack heights and uplift over rooftops (Abbot & Stedman 1999, AQMAU, 2016), however, these assumptions are clearly insufficient.

Returning to equation 5, the vertical ( $\sigma_z$ ) and horizontal ( $\sigma_y$ ) dispersion parameters reflective of the standard deviation in plume concentration, were calculated using Briggs-McElroy-Pooler functions for built-up areas (McElroy & Pooler 1968, Briggs 1973) and Pasquill-Gifford functions for flat rural locations (Turner 1970).

Dispersion parameters for unstable conditions (A and B stability classes) in urban settings, regardless of receptor distance, are calculated with (USEPA, 1995, p.33):

$$\sigma_z = 0.24x * (1 + 0.001x)^{-0.5} \quad (7a)$$

$$\sigma_y = \frac{0.32x}{(1 + 0.0004x)^{-0.5}} \quad (7b)$$

Dispersion parameters for unstable conditions (class A) in rural settings within 100m of the pollution source, are calculated with (USEPA, 1995, p.30–32):

$$\sigma_z = 122.8 * \left( \frac{x}{1000} \right)^{0.9447} \quad (8a)$$

$$\sigma_y = 465.1163 * \left( \frac{x}{1000} \right) * \tan \left( 0.0175 * 24.167 - \left[ 2.5334 * \log \left( \frac{x}{1000} \right) \right] \right) \quad (8b)$$

Where  $x$  is meters downwind distance from the source. A complete list of dispersion parameter functions by setting are provided in Appendix 14.

HADES uses the plume model to create a database of source specific (area, line, and point) dispersion kernels, for urban and rural locations, under all possible combinations of atmospheric condition. HADES considers 2,016 unique atmospheric combinations, based on 7 stability classes, 36 wind direction bands (by 10° increments), and across 8 wind speed groups (1, 2, 3, 4, 6, 8, 10, and 12 m/s). These dispersion kernels quantify how concentrations experienced at a central location are influenced by any nearby pollution source within a set search radius. The kernel matrices have a 10m x 10m resolution, and extend from the central location by 500m, 2km, and 4km for road-transport, area, and point sources, respectively.

The meteorological pre-processor (see section 2.2.3) then converts the hourly measurement data recorded at each weather station, into crosstabulations of wind speed, direction, and stability for the time period of interest (i.e., hourly-annual, seasonal, monthly, or weekly). By default, HADES constructs ‘hourly-annual average’ profiles ( $n = 24$ ). These profiles are then applied to the dispersion database, to create a series of weighted-average urban and rural source specific kernels for the location and time period of interest (see Appendices 15–17). The dispersion model in HADES is implemented via a ‘moving-window’ approach, where a source specific kernel reflective of the atmospheric conditions, centres on a receptor location, is multiplied with the corresponding cells of an emission grid, and then summed. A process known in GIS as focal statistics, or as convolution by image filtering applications. This grid-based approach allows for very fast processing of large numbers of emission sources, with no significant loss of detail in the underlying emission source geography.

For demonstration purposes, Fig. 2 displays the 24-hour annual average dispersion kernels for road-transport for the city of Nottingham. In this example, the prevailing south-westerly wind (typical for the UK) increases the influence of distant pollution sources from the south-west quadrant. Elevated concentrations are also associated with near-source contributions from gentle north-easterly winds (i.e., anticyclonic stagnation).

Weather stations are typically separated by tens of kilometres in urban locations, and by greater distances in predominantly rural locations. To model local dispersion processes, HADES implements the following procedure using sequentially profiled airshed release kernels (SPARK):

- Divide the study area into a series of 1km x 1km ‘airsheds’, each containing 100 receptor cells;
- Locate the three nearest weather stations to the centroid point of an airshed;
- Use ‘Inverse Distance Weighting’ (IDW) to calculate the geographic influence of each physical weather station on the airshed (i.e., triangulation to create a pseudo weather station).
- Create a time series of weighted-average dispersion kernels for a specified pollutant source in built-up (Urban Index = 1), and rural (Urban Index = 0) locations;

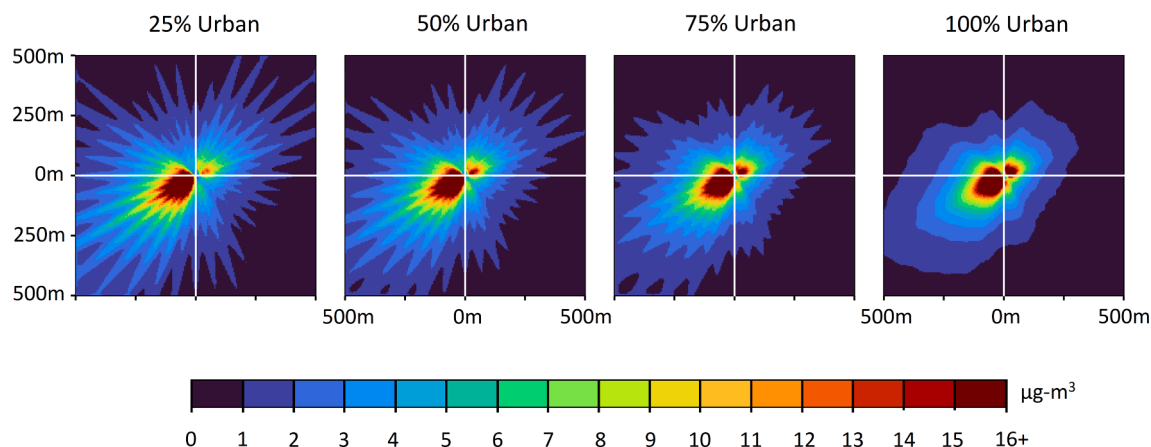


**Fig. 2.** Urban-rural variations in the annual average (24-hour) road-transportation dispersion kernels across Nottingham in 2019. These kernels record contributions to the central cell from NO<sub>x</sub> releases of 0.25 g per second, in each 10m x 10m cell within a 500m radius.

- e) Apply the convolution kernels to the hourly emission surfaces, and using the Urban Index fraction recorded at each location weight the time-series of exposure surfaces.

Typically, commercial dispersion modelling software uses a single weather to represent atmospheric conditions. An assumption that could result in model errors when dealing with large areas.

### 2.2.5. Topographic-atmospheric calibration

Model calibration was made using hourly measurement data from Defra, collected at sites used for compliance reporting in the Automatic Urban and Rural Network (AURN): <https://uk-air.defra.gov.uk/interactive-map>.

NO<sub>x</sub> contributions from the road-transport dispersion model (Fig. 1; SPARK) had a nonlinear (log-log) relationship with the measurement data. Whilst capturing the overall trend, the resulting concentrations were several orders lower than expected (Spearman's Rho = 0.75). Euro emission standard testing is known to underestimate real-world driving conditions, and there are other factors at play with local geometries influencing the containment and dispersion of pollution. Therefore, road-transport contributions are calibrated in accordance with urban driving conditions (reduced performance), building volume (containment), local elevation (dispersion), road/kerbside locations (slower plume release), and a minor temporal activity profile correction.

NO<sub>x</sub> contributions from the dispersion models of 'Point' (large industrial stacks) and 'Area' (i.e., commercial, domestic, other industrial, and natural) sources are combined and calibrated in accordance to urban environments (containment), deposition at elevated locations (likelihood of plume height equalling ground level), and a temporal activity profile correction.

Total NO<sub>x</sub> concentrations were therefore calculated by a three-stage process using measurement data from across England and Wales in 2018–19: (1) hourly-annual average atmospheric dispersion surfaces of road-transport were calibrated to 5,592 hourly-annual measurements at 120 kerbside and background locations; (2) domestic-commercial-industrial dispersion surfaces were calibrated to 3,480 measurements at 74 industrial and background locations; (3) the calibrated components enter a regression model with urban canyon parameters at all 129 measurement locations.

Topographic and atmospheric parameters are then used to model the photochemical reactions and pollutant sinks that determine the cyclic conversion of NO<sub>x</sub> to NO<sub>2</sub> and O<sub>3</sub> (Fig. 1; FIRE). All model variables are summarised in Appendix 1, with the full set of calibration and regression parameters provided for future applications in Appendices 18–22.

### 2.2.6. Modelling environment

HADES has been developed in the R programming language (version 4.3.1) using open-source scientific computing libraries for the parallel computation of spatial features and matrixes: doParallel, foreach, raster, and sf. HADES can compute 24 sets of hourly concentrations at 25 million discrete receptors (10m cells within a 50km x 50km study area) in less than 14 h on a High-Performance Computing system, with modest requirements: 14 threads (AMD EPYC 7002-Series processor) and 64 GB of memory implemented via SLURM. The Ordnance Survey separates the landmass of England and Wales into ninety-four 50km x 50km grids. By running jobs in parallel across all 128 available threads, it is possible to generate concentration surfaces across England and Wales within 1-week. Run times are linearly dependent on the number of receptors, and are unaffected by the number of emissions sources in the domain. In contrast, commercial Gaussian based pollution models are linearly dependent on both receptor and source counts, with expected city-scale run times in the order of several days/weeks.

### 2.3. Model evaluation

#### 2.3.1. Model performance

Model validation was undertaken by comparing predicted NO<sub>x</sub>, NO<sub>2</sub>, and O<sub>3</sub> hourly-annual average concentrations to up to 6,024 comparable measurements recorded at up to 136 locations across England and Wales in 2018–19. Extreme outliers within the hourly measurements of each pollutant were truncated prior to model development, defined as deviating from the median by three times the interquartile range (Tukey, 1977). Outlier analysis resulted in the truncation of 57 (0.9%) NO<sub>x</sub> and 17 (0.3%) NO<sub>2</sub> hourly-annual average measurements. The resulting NO<sub>x</sub>, NO<sub>2</sub>, and O<sub>3</sub> models in HADES were developed using concentrations ranging from 3.4 to 175.0 (IQR: 18.7–54.3), 3.3–80.0 (IQR: 14.2–29.8), and 14.6–74.7 (IQR: 40.6–56.5) µg/m<sup>3</sup>, respectively. Measurements of industry activity were limited to 9 locations (433 modelled hours), which recorded ground-level NO<sub>x</sub> and NO<sub>2</sub> concentrations ranging from 9.8 to 66.6 and 8.7–45.2 µg/m<sup>3</sup>. HADES has been developed to predict NO<sub>x</sub>, NO<sub>2</sub>, and O<sub>3</sub> concentrations up to values of 175 µg/m<sup>3</sup>, 80 µg/m<sup>3</sup>, and 80 µg/m<sup>3</sup>, respectively.

Model performance was assessed by goodness-of-fit (R-squared – R<sup>2</sup>; Pseudo-R-squared – PR<sup>2</sup>), residual (root mean squared error – RMSE; and RMSE normalised by the mean, range, or inter-percentile concentration range – NRMSE; overall and site-weighted mean average percentage error – MAPE), and chi-squared tests. PR<sup>2</sup> was included as the assumption of independent errors is violated in multilevel modelling. Thus, PR<sup>2</sup> tests the robustness of traditional goodness-of-fit tests with log-likelihood measures that should return comparable results where a valid model exists. Chi-squared log-likelihood ratios ensure that model

complexity is offset by gains in predictive power (where  $P < 0.05$ ): Validation with a Null (intercept only OLS) model, and if required, a second test confirms that the inclusion of hierarchical structures is appropriate (i.e., OLS vs multilevel model).

Performance tests were run on the base models and via cross-validation (CV) protocols. The first CV test was based on 10,000 Monte Carlo simulations, whereby 20% of the model's data was randomly withheld from the model development to be used in the model validation. A second CV test considered a new set of measurement data from 2020, to evaluate model robustness in an unusual scenario (i.e., during the 2020 COVID pandemic, draconian travel and workplace restrictions saw a radical redistribution and diminished levels of anthropogenic activities). HADES can account for uncertainty in its estimates based on either the 95% Confidence Interval (CI), or the 75% Highest Density Interval (HDI) of the Monte Carlo model development simulations (see Appendices 18-22).

### 2.3.2. Mapping and exposure assessment

HADES exposure surfaces of hourly-annual average ( $N = 24$ ) and annual average ( $N = 1$ )  $\text{NO}_2$  and  $\text{O}_3$  concentrations were created for England and Wales on a 10m x 10m grid for 2018–20. We also produced a statistical approximation of the annual-average daily maximum 8-hour rolling mean  $\text{O}_3$  concentration, calculated by combining the 24-hour mean with the standard deviation of the hourly annual-average surfaces ( $N = 24$ ). Exposures were calculated using two methods: (1) The 'Area-weighted' average of designated geographic zones, and (2) 'Population Weighted' exposures calculated from residential postcode delivery point locations, which on average represent the lived environment of 44 residents ( $SD = 39$ ) from 19 households ( $SD = 15$ ). Exposures were then summarised by nation, region, and community type, constructed from 188,880 UK Census Output Area community boundaries in 2021 (COA21). The Townsend Index (Townsend et al. 1989) was used to

describe community levels of relative socioeconomic deprivation in 2021 (Appendix 23), and the Urban Index appears to suitability convert into a traditional rural–urban classification scheme when averaged at a census community level (Appendix 24). We assessed exposure in relation to the current UK and EU legislative framework, and the 2021 air quality guidelines (AQG-2021) proposed by WHO.

## 3. Results

### 3.1. Summary of the source emission contributions

Total annual-average  $\text{NO}_x$  emissions across England and Wales in 2018, 2019, and 2020 were recorded at 677.8, 655.6, and 544.3 kilotonnes, respectively (Appendix 25). In 2018–19, large industrial stacks (traditional point sources), area sources, and road-transport individually accounted for 21.1%, 36.6%, 42.3% of the total primary  $\text{NO}_x$  emissions. Road-transport is the largest producer of  $\text{NO}_x$  and these emissions typically occur within lived environments where plume rises approximate human height. HADES estimates that road-transport is accountable for 76.3% of primary  $\text{NO}_x$  concentrations 1-meter above surface level, where the combined contribution of area and point source emissions equals that of road-transport (Appendix 20).

### 3.2. Model performance

Model performance and summary statistics for the prediction of hourly-annual  $\text{NO}_x$ ,  $\text{NO}_2$ , and  $\text{O}_3$  measurements in 2018–19 are summarised in Table 1. Cross-validation summary statistics are reported for the upper and lower 95% Highest Density Interval (95% HDI) of model simulations. For  $\text{NO}_x$  and  $\text{NO}_2$ , there were 124 measurements sites in 2018 and 127 in 2019, resulting in 6,024 site-hours (i.e., [24-hours x 124 sites] + [24-hours x 127 sites]) for hourly-annual-average and 251

**TABLE 1**  
HADES 2018–19 model performance and summary statistics for the prediction of  $\text{NO}_x$ ,  $\text{NO}_2$ , and  $\text{O}_3$ .

Summary Statistics			Hourly-Annual Average Concentration ( $\mu\text{g}/\text{m}^3$ )			Annual Average Concentration ( $\mu\text{g}/\text{m}^3$ )		
			Model 1: $\text{NO}_x$	Model 2: $\text{NO}_2$	Model 3: $\text{O}_3$	$\text{NO}_x$	$\text{NO}_2$	$\text{O}_3$
Description	Model Family	OLS	Multilevel	Multilevel	–	–	–	
	Model Relation	Linear	Linear	Linear	24-Hour Mean	24-Hour Mean	24-Hour Mean	
	Observations (N)	6,024	6,024	2,832	251	251	118	
Goodness-of-Fit	R-Squared ( $R^2$ )	0.71	0.79	0.89	0.72	0.80	0.86	
	Nagelkerke's Pseudo-R-Squared (PR2)	0.71	0.79	0.88	0.72	0.80	0.86	
Residuals *	Root Mean Square Error (RMSE)	18.01	5.63	3.76	15.52	4.90	3.17	
	Normalised RMSE (NRMSE <sub>RANGE</sub> )	10.5%	7.3%	6.2%	9.6%	6.9%	7.1%	
	Normalised RMSE (NRMSE <sub>IPR</sub> )	17.5%	14.3%	10.0%	16.9%	14.2%	11.4%	
	Normalised RMSE (NRMSE <sub>MEAN</sub> )	43.2%	24.4%	7.8%	37.2%	21.2%	6.6%	
	Mean Absolute Percentage Error (MAPE)	32.3%	18.4%	6.5%	29.7%	15.5%	5.3%	
	Site-Weighted MAPE (SW-MAPE)	13.1%	4.5%	3.4%	29.3%	14.8%	4.8%	
Chi-Square (p-value)	Full Model	< 0.01	< 0.01	< 0.01	< 0.01	< 0.01	< 0.01	
	Hierarchical Effects	–	< 0.01	< 0.01				
Cross-Validation (95% HDI) **	CV- $R^2$	Upper	0.71	0.79	0.89			
		Lower	0.68	0.77	0.87			
	CV-RMSE	Upper	18.02	5.67	3.82			
		Lower	16.81	5.33	3.63			
	CV-NRMSE <sub>RANGE</sub>	Upper	10.5%	7.4%	6.3%			
		Lower	9.8%	6.9%	6.0%			
Cross-Validation (2020 Dataset) ***	Observations (N)	3,072	3,068	1,416				
	CV- $R^2$	0.70	0.78	0.82				
	CV-RMSE	12.12	4.71	4.17				
	CV-NRMSE <sub>RANGE</sub>	8.7%	9.1%	7.5%				

\* NRMSE<sub>RANGE</sub> is the normalisation of the RMSE by the range of measured concentrations (max–min); NRMSE<sub>IPR</sub> is the normalisation of the RMSE by the inter-percentile (95th-5th) range of measured concentrations.

\*\* Cross-Validation (CV) was achieved by 10,000 Monte Carlo simulations, with 20% of the hourly data from 2018 to 19 randomly withheld from model development for use in model validation. Summary statistics from the 95% Highest Density Interval (HDI) of model simulations are presented.

\*\*\* CV was achieved by using the 2018–19 model to predict concentrations in 2020 (not seen by HADES). A linear calibration was applied to adjust the  $\text{NO}_x$  emission trend predicted by Model 1:  $\text{NO}_x = 0.841 + (\text{"Model 1"} \times 0.741)$ . Identical  $R^2$  values were reported without calibration, with reduced NRMSE<sub>RANGE</sub> values of 11.8% ( $\text{NO}_x$ ), 13.5% ( $\text{NO}_2$ ), and 8.6% ( $\text{O}_3$ ).

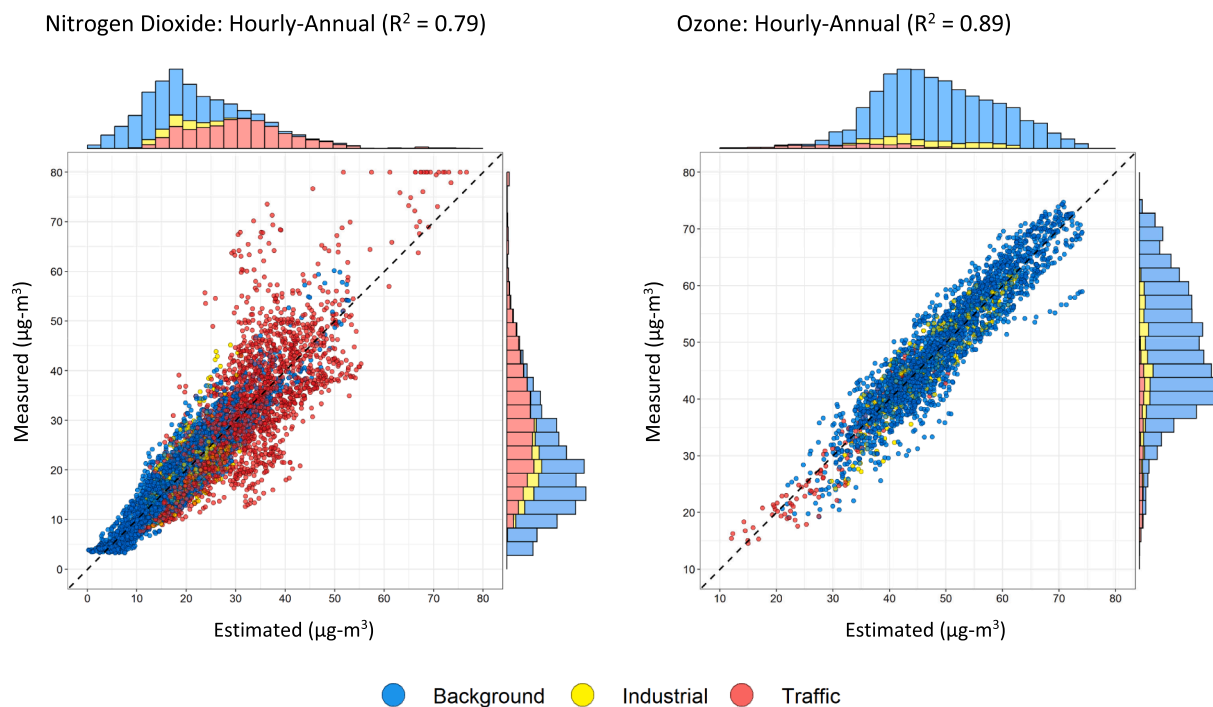


Fig. 3. Modelled (HADES) versus monitored hourly-average concentrations of nitrogen dioxide (NO<sub>2</sub>) and ozone (O<sub>3</sub>) in 2018–19.

sites for annual-average assessments. For O<sub>3</sub>, there were 60 measurements sites in 2018 and 58 in 2019, resulting in 2832 site-hours for hourly-average and 118 sites for annual-average assessments. Fig. 3 shows plots of measured versus predicted hourly-average NO<sub>2</sub> and O<sub>3</sub> (2018–2019), which were then aggregated into annual-average comparisons in Fig. 4.

Values of R<sup>2</sup> and PR<sup>2</sup> are within 1%, confirming model robustness. The NO<sub>x</sub> model explained 71% of the variation in the hourly-average measurement data. CV-R<sup>2</sup> values were 0.68–0.71 under Monte Carlo simulation and future prediction tests. The CV-RMSE was 16.8–18.0 µg/

m<sup>3</sup> across an observed NO<sub>x</sub> concentration range of 3.3 to 175 µg/m<sup>3</sup>. This equates to a 9.8–10.5% error in the estimates under the CV-NRMSE<sub>RANGE</sub> test (i.e., normalised by the range of measured concentrations). The NO<sub>2</sub> model explained 79% of the variation in the hourly-average concentrations with an RMSE of 5.6 µg/m<sup>3</sup>. In cross-validation, the NO<sub>2</sub> model explained 77–79% of the variation in the hourly-average measured concentrations at 129 locations, and RMSE between 5.3–5.7 µg/m<sup>3</sup>, across a NO<sub>2</sub> concentration range of 3.3 to 80 µg/m<sup>3</sup>. Overall NRMSE<sub>RANGE</sub> was 7.3% (95% HDI: 6.9–7.4%). The O<sub>3</sub> models explained 89% of the variation in measured concentrations in model

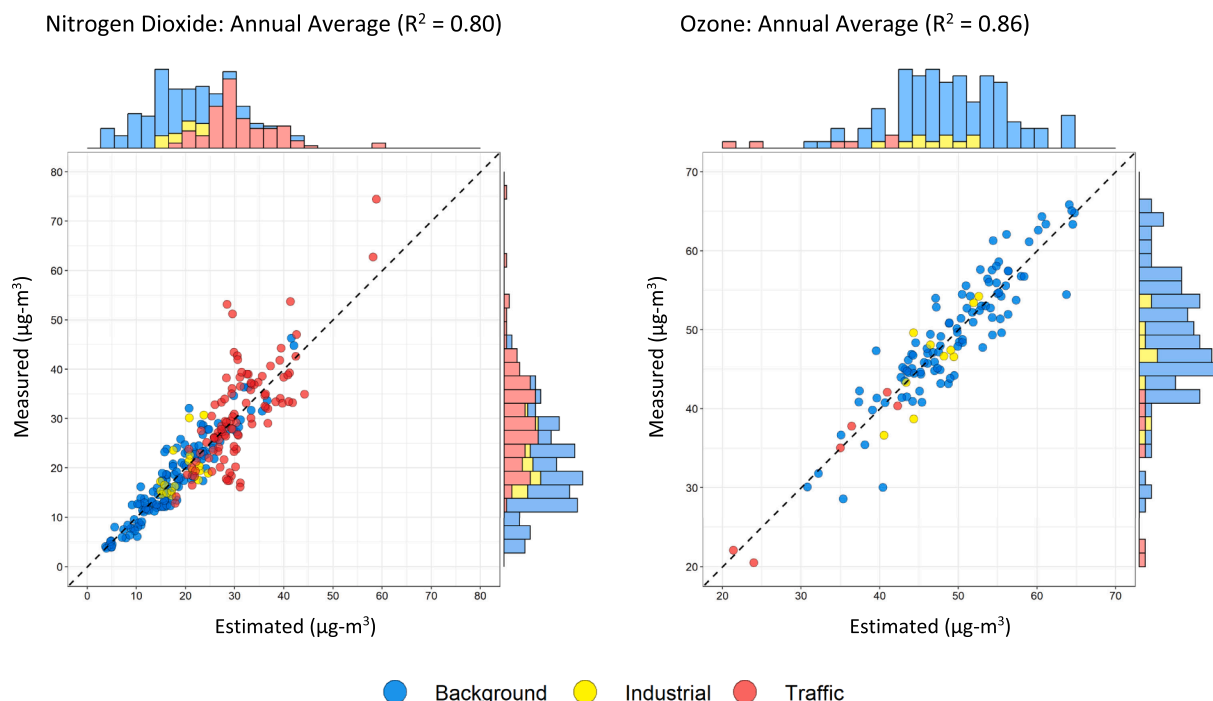


Fig. 4. Modelled (HADES) versus monitored annual average concentrations of nitrogen dioxide (NO<sub>2</sub>) and ozone (O<sub>3</sub>) in 2018–19.

fitting with an RMSE of  $3.8 \mu\text{g}/\text{m}^3$ . In cross-validation, the  $\text{O}_3$  model explained 87–89% of the variation in the hourly-annual measurement data at 60 locations with RMSE between  $3.6$ – $3.8 \mu\text{g}/\text{m}^3$ , across a  $\text{O}_3$  concentration range of  $14.5$  to  $74.7 \mu\text{g}/\text{m}^3$ . Overall  $\text{CV-NRMSE}_{\text{RANGE}}$  was 6.2% (95% HDI: 6.0–6.3%). The chi-squared tests show that the predictive power of all models has not been compromised by either the complexity of parameter or hierarchical structures ( $P < 0.05$ ).

Some variation in model performance was observed by time of day.  $R^2$  values calculated for each temporal subset of the hourly-annual average data (i.e., independently calculated for 01:00, 2:00, etc) were 0.68–0.76 and 0.70–0.87 for  $\text{NO}_2$  and  $\text{O}_3$ , respectively (Appendix 26).  $\text{NRMSE}_{\text{RANGE}}$  values for the hourly-annual average subsets returned relative errors of 6.4–9.6% for  $\text{NO}_2$ , and 7.2–10.1% for  $\text{O}_3$ . Diminished  $\text{NO}_2$  model performance ( $R^2 < 0.70$ ) appears restricted to the hours of 03:00 and 04:00, outside of periods of high activity and when concentrations are at their lowest. Diminished  $\text{O}_3$  model performance ( $R^2 < 0.80$ ) is restricted to the night-time period of 01:00 to 05:00. Likewise, the  $\text{NO}_x$  model performed best during peak activity hours ( $R^2 \geq 0.70$  from 07:00 to 19:00), reporting  $\text{NRMSE}_{\text{RANGE}}$  test errors of 7.7–13.4% over the course of a typical day.

Differences in model errors were seen by site type. The subsets of background, industrial and traffic (kerbside) measurement locations recorded MAPE values of 7.6%, 12.2%, and 26.4% in their  $\text{NO}_x$  predictions, respectively. The increased level of uncertainty at traffic sites is

due to the large variation in hourly  $\text{NO}_x$  measurements, which range from  $9.7$  to  $175 \mu\text{g}/\text{m}^3$  (IQR:  $37.4$  to  $84.7 \mu\text{g}/\text{m}^3$ ). Traffic sites account for 41% of the hourly observations in the model. The dispersion around the line of unity for  $\text{NO}_2$  concentrations (Fig. 3) reveals some sites, especially traffic sites, with relatively large errors. However, only 4.7% of site-hours had  $\text{NO}_2$  MAPE values  $> 50\%$ , with  $< 0.5\%$  of site-hours  $> 100\%$ . For  $\text{O}_3$ , there were only 3 site-hours (0.1%) where MAPE exceeded 50%. Values of site-weighted MAPE (Table 1) were notably lower for hourly-annual average concentrations, due to the reduced influence of traffic sites (i.e., for each site a single average absolute percentage error value is considered, rather than up to 48 hourly-annual average values over the 2-years).

The  $\text{NO}_x$  model explained 72% of the variation in the annual average measured concentrations, with an  $\text{NRMSE}_{\text{RANGE}}$  of 9.6% (Table 1). The  $\text{NO}_2$  model explained 80% of the variation in the annual average measured concentrations with an RMSE of  $4.9 \mu\text{g}/\text{m}^3$  and  $\text{NRMSE}_{\text{RANGE}}$  of 6.9% (see Table 1 and Fig. 4). The  $\text{O}_3$  model explained 86% of the variation in the annual average measured concentrations, with a RMSE of  $3.2 \mu\text{g}/\text{m}^3$  and  $\text{NRMSE}_{\text{RANGE}}$  of 7.1%. Values of RMSE and  $\text{NRMSE}_{\text{RANGE}}$  are comparable to the hourly-annual assessments. For annual average concentrations, predictions at all sites were within 100% MAPE for both  $\text{NO}_2$  and  $\text{O}_3$ . Predictions at 5 sites were greater than 50% MAPE for  $\text{NO}_2$  but all  $\text{O}_3$  predictions were less than 50% MAPE.

HADES was robust to the unexpected emissions scenarios related to

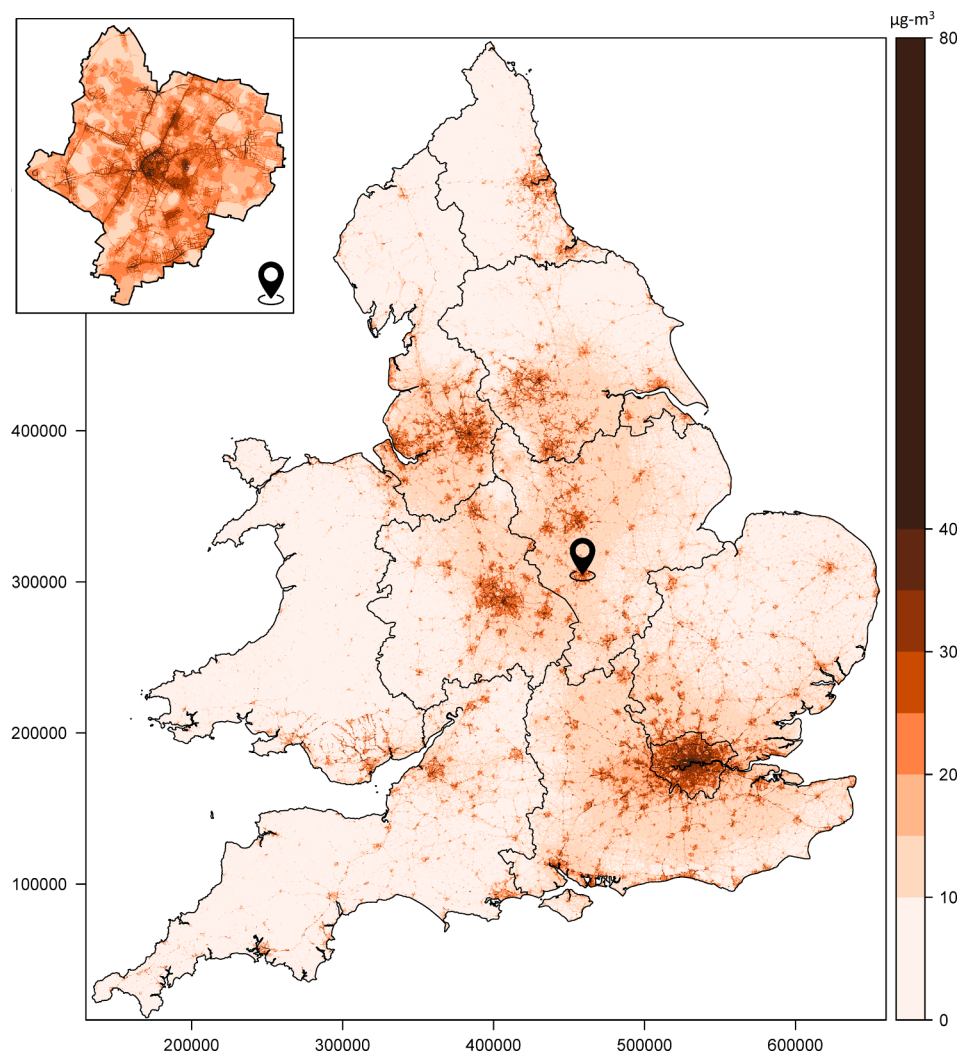


Fig. 5. Annual average (24-hour) nitrogen dioxide concentrations across England and Wales in 2018–19. Insert displays the City of Leicester located within the East Midlands region.

TABLE 2

Population-Weighted annual-average residential exposures across England and Wales. Constructed from 1,377,387 postcode centroids, which on average represent the lived environment of 44 residents (SD = 39) in 19 households (SD = 15).

Scheme	Group	Population	Annual-Average Concentrations ( $\mu\text{g}/\text{m}^3$ )								
			24-Hour NO <sub>2</sub>			24-Hour O <sub>3</sub>			8-Hour O <sub>3</sub> *		
			2018	2019	2020	2018	2019	2020	2018	2019	2020
National	All	100%	18.2	20.2	17.0	49.1	46.9	51.4	56.7	54.4	59.1
	England	95%	18.5	20.5	17.3	48.8	46.6	51.1	56.4	54.2	58.9
	Wales	5%	13.7	14.6	12.3	54.0	53.0	56.0	60.5	59.8	62.8
Rural-Urban	Urban	66%	20.1	22.2	18.6	47.8	45.5	50.4	55.4	53.1	58.2
	Peri-Urban	12%	16.9	18.6	15.8	49.7	47.7	51.9	57.1	55.0	59.5
	Peri-Rural	9%	15.4	17.1	14.6	50.8	48.8	52.7	58.2	56.1	60.2
	Rural	13%	12.0	13.5	11.8	53.9	52.0	55.2	61.5	59.4	62.9
Regional	East Midlands	8%	17.8	19.6	17.0	48.2	46.0	50.5	55.8	53.0	58.1
	East England	11%	16.6	18.2	15.9	49.5	47.9	51.6	57.9	56.2	60.4
	London	15%	25.3	29.0	24.1	44.9	41.2	47.6	53.3	49.8	56.3
	North East	4%	16.8	15.7	14.7	48.7	50.5	52.9	54.5	56.2	58.8
	North West	12%	18.9	20.9	17.2	49.0	45.3	50.6	56.0	51.7	57.5
	South East	16%	17.6	20.0	16.4	49.7	47.0	51.8	57.8	55.8	60.4
	South West	10%	13.4	14.9	12.6	53.6	52.0	55.1	61.0	60.0	62.7
	Wales	5%	13.7	14.6	12.3	54.0	53.0	56.0	60.5	59.8	62.8
	West Midlands	10%	18.3	20.1	17.1	49.1	46.8	51.9	56.9	53.8	59.4
	Yorkshire & The Humber	9%	17.5	18.9	16.3	48.0	47.2	50.7	54.7	53.4	57.2
Deprivation (Quantiles)	Q1: Affluent	20%	15.6	17.2	14.8	51.1	49.0	52.9	58.7	56.4	60.6
	Q2	20%	16.1	17.8	15.2	50.7	48.7	52.7	58.3	56.3	60.5
	Q3: Expected	20%	17.6	19.4	16.4	49.5	47.5	51.8	57.1	55.1	59.6
	Q4	20%	19.4	21.3	17.9	48.2	46.0	50.7	55.8	53.5	58.5
	Q5: Deprived	20%	22.4	24.8	20.8	46.1	43.4	48.9	53.7	50.9	56.7

\* Statistical approximation of the annual-average daily maximum 8-hour rolling mean ozone concentration, calculated by combining the mean with the standard deviation of the hourly annual-average surfaces ( $n = 24$ ).

the COVID pandemic, predicting across the nitrogen cycle in 2020 with minimal diminishment in performance: The NO<sub>x</sub>, NO<sub>2</sub>, and O<sub>3</sub> models explained 70%, 78%, and 82% of the variation in the hourly-annual average measurements, respectively. Calibration of NO<sub>x</sub> (Model 1) via linear regression against measured concentrations for 2020, prior to the calculation of NO<sub>2</sub> (Model 2) and O<sub>3</sub> (Model 3) further reduced model errors in this unusual year: NRMSE<sub>RANGE</sub> modelling errors were reduced from 13.5% to 9.1% for NO<sub>2</sub>, and from 8.6% to 7.5% for O<sub>3</sub>. Appendices 27–28 summarise the performance of the preliminary calibration models and the total NO<sub>x</sub> emission model on the 2018–19 training data, and for forecasting concentrations in 2020.

### 3.3. National exposure assessment (2018–19)

Fig. 5 shows the annual average NO<sub>2</sub> concentration surface for 2018 and 2019 (combined), with the legend marking related to the current UK and EU annual limit of 40  $\mu\text{g}/\text{m}^3$  set in 2010 (EC, 2008), and the recently proposed AQG-2021 of 10  $\mu\text{g}/\text{m}^3$  (WHO 2021). Appendix 29 shows the equivalent surface for O<sub>3</sub>. To support their interpretation, Table 2 contains population-weighted exposures at residential postcode delivery point locations and Appendices 30–31 provide area-weighted exposures by nation, region, and community area type.

Area-weighted (or background) NO<sub>2</sub> concentrations of 8.6–9.9  $\mu\text{g}/\text{m}^3$  were estimated across England and Wales in 2018–19. A clear urban–rural divide exists with, urban community spaces typically experiencing concentrations of 19.3–21.1  $\mu\text{g}/\text{m}^3$ , levels that are twice as high as their rural counterparts. Rural areas constitute approximately 89% of the overall land mass, but contain a relatively small proportion of the population. Area-weighted NO<sub>2</sub> concentrations of 22.3–25.9  $\mu\text{g}/\text{m}^3$  within London, are twice as high as the South-East region that borders the capital. A clear social divide is also observed, with land across deprived communities typically experiencing NO<sub>2</sub> concentrations that are 11.4–12.3  $\mu\text{g}/\text{m}^3$  higher than affluent spaces. In terms of legislative compliance, <0.1% of the England and Wales landmass currently exceeds the 40  $\mu\text{g}/\text{m}^3$  limit, with 64.5% of the land meeting the proposed AQG-2021 of 10  $\mu\text{g}/\text{m}^3$ .

It is estimated that 66%, 21% and 13% of the population respectively live in urban, suburban, and rural locations (Table 2). As such, the typical residential annual-mean exposure to NO<sub>2</sub> across England and Wales in 2018–19 is estimated at a substantially higher concentration of 18.2–20.2  $\mu\text{g}/\text{m}^3$ . Typically, exposures at residential locations are noticeably higher than across community spaces, differing by 1  $\mu\text{g}/\text{m}^3$  in urban and 4.5  $\mu\text{g}/\text{m}^3$  in rural locations. In terms of legislative compliance, 0.2% of the population for England and Wales reside in locations exceeding the 40  $\mu\text{g}/\text{m}^3$  limit, with only 4.3% of the population housed in locations exposed to  $\leq 10 \mu\text{g}/\text{m}^3$ . Based on these results, meeting the AQG-2021 is a major challenge for NO<sub>2</sub> exposure.

Fig. 6 shows hourly-annual average NO<sub>2</sub> concentrations at selected (3-hourly) time intervals across the day, and the annual average for the city of Leicester in 2018–19, as an example of the capability of the modelling in terms of spatial and temporal resolution. Concentrations above 40  $\mu\text{g}/\text{m}^3$  appear limited to a few kerbside locations and are heavily influenced by commuter patterns (Appendix 32).

O<sub>3</sub> is a regional pollutant that tends to reach high concentrations far from pollutant sources during prolonged warmer periods. Within the UK, modelled annual-average levels of O<sub>3</sub> for 2018–19 did not exceed 75  $\mu\text{g}/\text{m}^3$ , with <0.1%, 72.7%, and 27.3% of the landmass respectively reported concentrations <30, 30–60, and >60  $\mu\text{g}/\text{m}^3$ . These O<sub>3</sub> levels are considerably lower than any prescribed safety limit for immediate risk to the general population. Legislative health-based limits for O<sub>3</sub> are set around a maximum daily 8-hour rolling mean of 120  $\mu\text{g}/\text{m}^3$ , not to be exceeded for >25 days per year (EC 2008). All 78 monitoring sites across the UK were compliant throughout 2018 and 2019, recording on average only 5 days of exceedance.

AQG-2021 has recommended additional compliance with a 60  $\mu\text{g}/\text{m}^3$  peak-season (6-month) average daily maximum 8-hour mean O<sub>3</sub> concentration. We conservatively benchmark against this standard using a statistical approximation of the annual-average maximum daily 8-hour rolling mean (see Table 2 and Appendix 33). Only the South-West and Wales have regional population-weighted exposures that exceed 60  $\mu\text{g}/\text{m}^3$ . In total, 15.2% of the population across England and Wales reside in locations expected to exceed this guideline. Area-weighted exposures

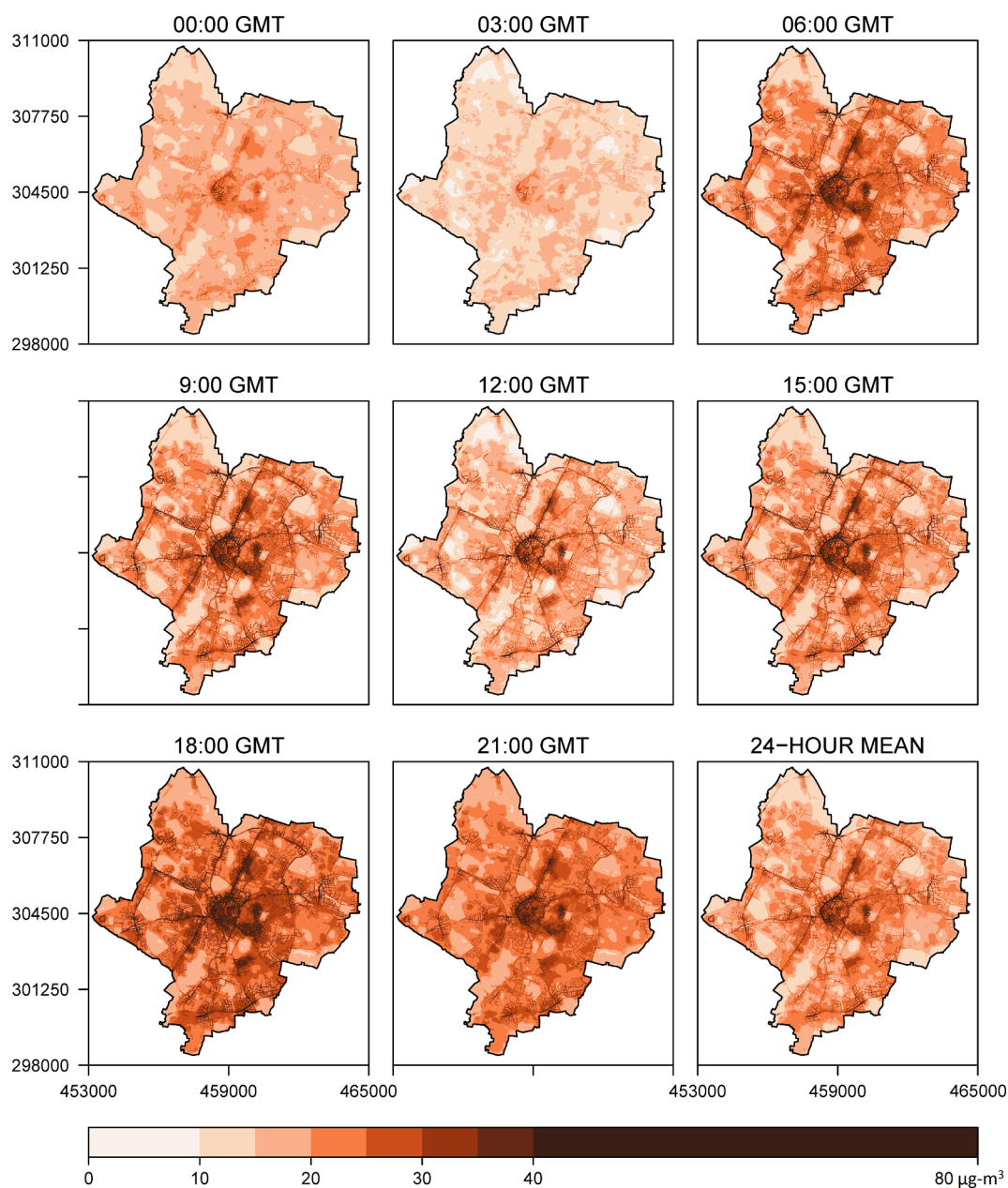


**Fig. 6.** Hourly annual-average nitrogen dioxide concentrations across Leicester in 2018–19, projected in the British National Grid coordinate system (10 m resolution).

indicate that most rural and affluent community spaces will exceed such guidelines (Appendix 30). It is important to note that this AQG-2021 only considers the warmest 6-months of a year; our analysis covers 12-months and therefore likely underestimates the level of exceedance for  $O_3$ .

### 3.4. Covid-19 interventions in 2020

The pandemic ‘lockdown’ policies led to the temporary closure (or ‘mothballing’) of many industrial and commercial premises, and the restriction of travel to varying degrees throughout the year.

In 2020,  $NO_x$  concentrations across England and Wales fell by 22.0% (Appendix 31). Across Great Britain, reductions in road traffic of 23–25% and 18% were reported on major and minor roads, respectively (Appendix 34). This corresponded to a 22.6% reduction in  $NO_x$  emissions across the entire 351,573 km road network in England and Wales.

$NO_x$  emissions from ‘Area’ sources fell by 19.3%, whereas large industrial ‘Point’ source emissions only fell by 1% on 2019 levels (Appendix 25). Activity at large industrial operations varied by region, reducing by 18.3% in the East Midlands, and increasing by >20% in London and the South West. Non-road transport (i.e., air, rail, and waterways), small-medium industrial activity, and domestic-commercial heating typically account for 42.4%, 25.7%, and 21.2% of ‘Area’ source  $NO_x$  emissions – activity in these sectors fell by 23.6%, 19.3%, and 12.2%, respectively (Appendix 35).

However, this overall reduction and redistribution of polluting activities only corresponded to a 5.9% fall in  $NO_2$  concentrations, and a 3.3% increase in  $O_3$  concentrations was observed across 2020 (Table 2). Modest ‘improvements’ in overall air quality, disproportionate to the reduction in polluting activities were previously reported for the initial pandemic ‘lockdown’ in the Spring of 2020, largely offset by changes in the local atmospheric chemistry and weather events (Jephcote et al

2021).

In London, average air temperatures across 2020 were 0.3°C higher than in 2019, there was an 8% increase in heatwave events (hourly records >20°C), and high-pressure weather systems associated with northeasterly winds were more prevalent (Appendix 36). Therefore, the 29.1% reduction in NO<sub>x</sub> across London in 2020 coincided with only a 11.2% reduction in NO<sub>2</sub>, and an unusual 9.4% increase in O<sub>3</sub> because of favourable weather conditions and limited street level emissions entering the nitrogen cycle (Appendix 30). Similar trends were observed in many urban environments. Appendix 37 shows the mapped percentage change in annual average NO<sub>2</sub> and O<sub>3</sub> concentrations for 2020, with respect to modelled concentrations in 2018–19 across England and Wales. The exact location, extent, and magnitude of this anthropogenic change was previously unknown, restricted to the analysis of select monitoring sites or regional satellite-based models.

The NO<sub>2</sub> and O<sub>3</sub> models explained 78% and 82% of the variation in the overall set of hourly-annual average measurements in 2020, respectively. R<sup>2</sup> values calculated for each subset of the hourly-annual average data were 0.63–0.79 and 0.57–0.77 for NO<sub>2</sub> and O<sub>3</sub>, respectively. NRMSE<sub>RANGE</sub> values for the hourly-annual average subsets returned relative errors of 10.1–14.4% for NO<sub>2</sub>, and 9.1–13.8% for O<sub>3</sub>.

#### 4. Discussion

We produced a new approach to air pollution modelling (HADES) that combines the dispersion modelling (of a detailed source emissions inventory), satellite observations, and other topographical data, within a statistical calibration framework. We demonstrated HADES for hourly-annual and annual average concentrations mapping (10m surfaces) and exposure assessment. We have made the concentration surfaces for England and Wales open access for non-commercial use (see ‘Availability of Data’). We believe these to be the most accurate, freely available national-scale surfaces within the UK that reflect the influence of meteorology on patterns of air pollution. The methods and supplementary materials (Appendices and traffic emission toolkit) provide detailed guidance for others wishing to employ HADES, including the generation of synthetic data where required. HADES is an efficient dispersion model that facilitates the rapid (i.e., compared to previous approaches including dispersion modelling) production of national-scale air pollution maps.

##### 4.1. Comparison of model performance with other studies

National-scale studies have mostly used statistical modelling based in around LUR (Ma et al., 2024) with a few exceptions, as noted earlier (Klompemaker et al., 2021). Earlier LUR studies were limited to topographical variables to represent proximity to air pollution source and sinks (Hoek et al., 2008). Satellite data and/or chemical transport models are increasingly included in modelling as a source of background concentrations alongside topographical data, and have been referred to as ‘hybrid’ approaches (de Hoogh et al., 2018). We believe our national-scale hybrid model including dispersion modelling, satellite data, and topographical data in a statistical calibration to be unique.

In terms of the performance of national models, Novotny et al. (2011a), Novotny et al. (2011b) satellite-derived 30m LUR models for the USA, explained 72% of the variation in annual average NO<sub>2</sub> surface concentrations. National LUR models for China and Australia using satellite products and meteorological data, report R<sup>2</sup> values ranging from 0.73 to 0.81 for NO<sub>2</sub> (Xu et al., 2019; Knibbs et al., 2014). Compared to other approaches our annual average predictions had excellent performance: R<sup>2</sup> of 0.80 for NO<sub>2</sub> and R<sup>2</sup> of 0.86 for O<sub>3</sub> in relation to measurements made in 2018–2019. As far as we are aware, there are no studies to have reported performance of hourly-annual average models. Our models had similar overall performance between hourly annual and annual average models.

Many studies report RMSE (the average difference between

predictions and measurements), but values are difficult to compare due to differences in measured concentration variability between study areas. NRMSE allows comparison, however, normalisation may use the mean, range, IQR, or percentile. In Great Britain, NO<sub>2</sub> LUR models for 2009 reported a NRMSE<sub>MEAN</sub> of 34%, NRMSE<sub>RANGE</sub> of 12%, and NRMSE<sub>IPR</sub> of 20% (Gulliver et al., 2013). Models for 2011–2015 report a NRMSE<sub>MEAN</sub> of 25–27%, NRMSE<sub>RANGE</sub> of 13–14%, and NRMSE<sub>IPR</sub> of 8% for NO<sub>2</sub>, and a NRMSE<sub>MEAN</sub> of 7–10%, NRMSE<sub>RANGE</sub> of 6–11%, and NRMSE<sub>IPR</sub> of 10–16% for ozone (Wang et al., 2022). Across Western-Europe, LUR models yielded a NRMSE<sub>MEAN</sub> of 35% and NRMSE<sub>IPR</sub> of 21% for NO<sub>2</sub>, and NRMSE<sub>MEAN</sub> of 10% and NRMSE<sub>IPR</sub> of 18% for annual average O<sub>3</sub> (de Hoogh et al., 2018). In the Netherlands, LUR O<sub>3</sub> models reported a NRMSE<sub>MEAN</sub> of 10% and NRMSE<sub>RANGE</sub> of 15% (Kerckhoffs et al., 2015). In the USA, Lu et al. (2021) reported NRMSE<sub>MEAN</sub> ranges of 29–33% and 8–9% for NO<sub>2</sub> and O<sub>3</sub>, respectively. HADES recorded a NRMSE<sub>MEAN</sub> of 21%, NRMSE<sub>RANGE</sub> of 7%, and NRMSE<sub>IPR</sub> of 14% for NO<sub>2</sub>, and a NRMSE<sub>MEAN</sub> of 7%, NRMSE<sub>RANGE</sub> of 7%, and NRMSE<sub>IPR</sub> of 11% for O<sub>3</sub> (Table 2). Our results are favourable compared to the results from other studies, but a robust assessment would require comparison between different methods using the same measurement data.

##### 4.2. Applying hades to other locations

HADES was developed to allow the use of open-access input data with potentially near-global coverage. As noted above in describing the various input data, many of the required datasets (e.g., population, topography, land use, area-level emissions data), are readily available and sufficiently detailed to apply HADES elsewhere. The main exception to this is data on road traffic flows. To fill this gap is challenging as detailed traffic datasets are not common, even for major roads in many countries. Traffic count data is available commercially but is prohibitively expensive for academic research and the public sector. Applying traffic assignment modelling (Kučera and Chocholáč, 2021) at national scale is not computationally feasible for this exercise. There is, however, a growing body of studies that have shown statistical models of traffic flows to be promising. Most examples so far have been for individual cities or regions (Apronti et al., 2016; Sfyridis and Agnolucci, 2023; Alvarado-Molina et al., 2023) but also nationally (Morley & Gulliver, 2016), and more recently the first international-scale model, for Europe (Shen et al., 2024). To produce data on road traffic speed, we suggest using national speed limits by road type described above, which can be determined by OSM road types by country.

As is the case in our application for England and Wales, we don't expect data to be available for other explicit sources (i.e., depicted by individual points or areas), except for major industrial installations such as power plants. It is assumed therefore that most domestic and industrial emissions sources will be summarised on a grid and treated in HADES as a diffuse source. For England and Wales this data is published on a 1km grid; also available for the rest of the UK. For other countries, where these data are only available nationally or regionally by sector (e.g., in EMEP) it is theoretically possible to get an estimate of emissions on a suitable grid by disaggregating the emissions totals using a form of areal weighting (e.g., weighted by population density). In this presentation, we applied a land use informed disaggregation approach to a 10m grid for modelling for each emissions sector. This relates well to the spatial resolution of discrete emissions sources such as road links or industrial point or area sources, but we recognise that 10m is a ‘false resolution’ imposed on the 1km gridded emissions used here. We also rendered the data used in the statistical calibration (e.g., CAMS surfaces, land use, population) component of HADES to a 10m grid. It makes sense from a modelling perspective, however, to run HADES using a consistent grid that reflects the scale of the most detailed source(s) to prevent increased levels of uncertainty. We chose CAMS data to represent long-range transportation of air pollutants, and it's (regional and international) influence on background concentrations in HADES, but other datasets are suggested in section 2.1.4 for global application.

#### 4.3. Alternative approaches

There has been a rise in recent years in the number of studies using machine learning, especially tree-based (e.g., random forest, extreme gradient boosting, and stochastic gradient boosting) as well as other types of method (e.g., support vector regression, neural networks, and kernel-based regularised least squares). In a recent study (Vachon et al., 2024) tree-based methods performed the best in 12 out of 17 multi-model comparisons. However, one of the main weaknesses of tree-based methods is that they are constrained to predicting values within the range of observed values (Vachon et al., 2024). Machine learning, as with other statistical methods, can also suffer from overfitting and may not transfer well to other locations (Tang et al., 2024). Even where models are trained on concentration data from hundreds of measurement locations this does not ensure out-of-sample representativeness, even following held-out validation or extensive cross-validation. A further limitation of machine learning is that it cannot be directly used for assessing interventions, unlike with dispersion modelling where it is possible to change emissions within a source sector and study the impact on changes in air pollution surfaces. Thus, approaches incorporating dispersion modelling provide a stronger basis for interpretability. Another advantage of HADES, and dispersion modelling in general, is that the patterns of air pollution reflect the effects of meteorology. Some statistical methods have applied pseudo meteorological variables such as wind terms (Naughton et al., 2018) but these represent a simplification of the relationship between meteorology and atmospheric processes.

Despite some shortcomings, however, machine learning and other statistical approaches (e.g., stepwise regression, generalised additive mixed models, etc.) offer an accessible method for producing air pollution surfaces where detailed information on emissions is not available and there is a sufficiently detailed series of concentration measurements sites. Machine learning may offer a faster means of producing air pollution estimates than HADES. Statistical methods are a popular choice in epidemiological research (Jie et al., 2021), especially where relative ranking of exposures may be more important than absolute accuracy.

#### 4.4. Limitations and future work

As part of a hybrid approach, we included 3-D building data as a GIS surrogate (i.e., street canyon) for the effect of ventilation on pollutant dispersion. Buildings were used in the statistical calibration, as it would not be practical to produce a physical model of the effects of buildings at national scale. In modelling concentrations of NO<sub>x</sub> for London, Masey et al. (2018) compared the performance of GIS surrogates, including sky-view factor (i.e., amount of sky visible from each location), following Eeftens et al. (2013), with established street canyon models: the STREET model (Johnson et al., 1973) and the AEOLIUS Model (Vardoulakis et al., 2002). Although the street canyon models provided slightly lower bias at fixed site monitoring locations within street canyons, there was little difference between modelled and measured concentrations of NO<sub>x</sub> when all types of receptor locations were considered. Qi et al. (2022) present novel methods for constructing GIS surrogates of street configurations via google street imagery in two cities in the USA which although promising are currently impractical for nationwide applications.

Reduced model performance was observed at some traffic (kerbside) locations, but these represented a small part of dataset. Kerbside concentrations are difficult to capture due to their high levels of spatio-temporal variability (i.e., NO<sub>x</sub> ranges from 9.7 to 175 µg/m<sup>3</sup>) and immediate proximity to the source. The increased error at these traffic sites may relate to relatively weak performance of the traffic flow model at specific locations, which future research will seek to address. Indeed, 7.5% of the hourly-annual average NO<sub>2</sub> estimates at traffic locations had MAPE values above 50%.

At present, HADES outputs are limited to annual average assessments (hourly and 24-hour) for NO<sub>x</sub>, NO<sub>2</sub> and O<sub>3</sub> across England and Wales. We intend to extend the modelling to the rest of the UK (Scotland and Northern Ireland) and develop modelling capacity for fine particulates with the additional consideration of non-tailpipe emissions and background concentrations of PM<sub>2.5</sub> (i.e., chemistry and secondary particle formation). Periods of interest for finer temporal assessments may include seasons, or specific months of the year for studies of pregnancy and infancy in epidemiologic research. It is unlikely that we or others will be able to obtain reliable estimates of the seasonal variability in local-scale sources emissions to support deterministic modelling for sub-annual averaging periods. A more realistic approach would be to either include statistical terms for the combinations of hour, day and month in the FIRE 'regression calibration' component of HADES (see Fig. 1), or calibrate the annual-average model output using sub-annual (e.g., daily or monthly) concentrations from monitoring networks as others have shown (Ndiaye et al., 2024).

All environmental modelling applications are limited by the spatial accuracy and precision of the emission data that underpins them. HADES contains its own traffic modelling platform, which applies detailed and established speed-based emission testing functions to observation-informed models of traffic activity at a high spatial resolution. Operational records for large industrial stacks ('Point' sources) are also typically well maintained to ensure compliance with environmental regulation. Uncertainty can exist in the 'Area' source data, where the location and extent of individual activities may be missing, and when sector contributions are based on national or regional level estimates. Such uncertainty is difficult to account for and is often overlooked in the construction of the emission data and by environmental models. HADES has been developed with Monte Carlo simulation and can therefore account for overall uncertainty (not source specific) in its estimates of NO<sub>x</sub>, NO<sub>2</sub>, and O<sub>3</sub> through using the 95% CI and 75% HDI regression parameters provided in Appendices 20-22.

The 2018–20 national pollution surfaces will be used to improve the exposure records of two major biomedical databases: (1) UK Longitudinal Linkage Collaboration containing participants from 20 cohorts, and (2) The UK Biobank containing >475,000 participants. HADES may be used to explore pollutant exposures beyond the legislative requirements of annual average concentrations. This is useful from a policy perspective to understand why exceedances may occur, and from an epidemiological perspective to: (a) replace residential with activity-weighted exposures minimising issues of misclassification, and (b) coincide with other time dependent exposures such as noise pollution.

#### 4.5. Air quality guidelines and policy support

Our study represents a comprehensive analysis of long-term air pollutant exposures conducted for England and Wales, with pollutant exposures estimated at >1.5 billion locations for mapping. For context, the UK governments 1km x 1km annual background pollutant maps only consist of 154,649 land cells in England and Wales, a resolution which raises concerns of severe exposure misclassification. We suggest that our model output may be used for research and policy support in the UK, including health impact assessment. The modelling framework could be applied elsewhere for the same purposes. Our analysis has shown that many areas in England and Wales would not meet the WHO AQG-2021 for NO<sub>2</sub>. The AQG-2021 for maximum 8-hour average ozone may also not be met in many places, especially in suburban and rural areas. Although not currently adopted as air quality targets in the UK, the AQG-2021 represents a major challenge for outdoor air quality.

#### Funding sources

The development of HADES did not receive any specific grant from funding agencies in the public, commercial, or not-for-profit sectors.

The creation of the national exposure surfaces for England and

Wales, and the open access publication of the modelling framework, was funded by UK Research and Innovation and the Medical Research Council (Grant ID: MC\_PC\_20030).

### CRedit authorship contribution statement

**Calvin Jephcote:** Writing – review & editing, Writing – original draft, Visualization, Validation, Software, Resources, Methodology, Investigation, Formal analysis, Data curation, Conceptualization. **John Gulliver:** Writing – review & editing, Writing – original draft, Visualization, Validation, Resources, Methodology, Formal analysis, Conceptualization.

### Declaration of competing interest

The authors declare that they have no known competing financial interests or personal relationships that could have appeared to influence the work reported in this paper.

### Acknowledgements

We would like to thank the following data providers for their creation of open access data repositories, which have enabled us to develop this air pollution modelling framework: Copernicus Atmosphere Monitoring Service (CAMS), European Environment Agency (EEA), UK Department for Business, Energy & Industrial Strategy (BEIS), UK Department for Environment, Food & Rural Affairs (DEFRA), UK Department for Transport (DfT), US National Oceanic and Atmospheric Administration (NOAA), and the WorldPop service.

This research used the ‘ALICE-3 High Performance Computing Facility’ at the University of Leicester. For the purpose of open access, the author has applied a Creative Commons Attribution license (CC BY 4.0) to any Author Accepted Manuscript version arising from this submission.

### Supplementary Data

Supplementary data to this article can be found online at <https://doi.org/10.1016/j.envint.2025.109304>.

### Data availability

A Figshare repository contains the annual average nitrogen dioxide (NO<sub>2</sub>) and ozone (O<sub>3</sub>) concentration surfaces for England and Wales in 2018–2020, available as open access for non-commercial use (CC BY-NC 4.0): <https://doi.org/10.6084/m9.figshare.27073906>.

### References

- Abbot, J., Stedman, J., 1999. Dispersion modelling and mapping studies for review and assessment of PM<sub>10</sub>. Department of the Environment, Transport and the Regions. AEAT-, Oxford, UK. Report, p. 5273.
- Air Quality Modelling & Assessment Unit (AQMAU), 2016. Diesel generator short term NO<sub>2</sub> impact assessment. UK Environment Agency. Report: AQMAU-C1457-RP01.
- Alduchov, O.A., Eskridge, R.E., 1996. Improved Magnus Form Approximation of Saturation Vapor Pressure. *J. Appl. Meteorol.* (1988–2005) 35 (4), 601–609. [https://doi.org/10.1175/1520-0450\(1996\)035<0601:IMFAOS>2.0.CO;2](https://doi.org/10.1175/1520-0450(1996)035<0601:IMFAOS>2.0.CO;2).
- Alvarado-Molina, M., Curto, A., Wheeler, A.J., Tham, R., Cerin, E., Nieuwenhuijsen, M., Vermeulen, R., Donaire-Gonzalez, D., 2023. Improving traffic-related air pollution estimates by modelling minor road traffic volumes. *Environ. Pollut.* 338, 122657.
- Apronti, D., Ksaibati, K., Gerow, K., Hepner, J.J., 2016. Estimating traffic volume on Wyoming low volume roads using linear and logistic regression methods. *Journal of Traffic and Transportation Engineering (English Edition)* 3 (6), 493–506.
- Briggs, G.A., 1973. Diffusion Estimation for Small Emissions. ATDL Contributions File No. (Draft) 79. Air Resources Atmospheric Turbulence and Diffusion Laboratory. National Oceanic and Atmospheric Administration, Oak Ridge.
- Brauer, M., Brook, J.R., Christidis, T., Chu, Y., Crouse, D.L., Erickson, A., Hystad, P., Li, C., Martin, R.V., Meng, J., Pappin, A.J., Pinault, L.L., Tjepkema, M., van Donkelaar, A., Weagle, C., Weichenthal, S., Burnett, R.T., 2022. (2022) ‘Mortality-Air Pollution Associations in Low Exposure Environments (MAPLE): Phase 2’. Research Report (health Effects Institute) 212, 1–91.
- Brunekreef, B., Holgate, S.T., 2002. Air pollution and health. *Lancet (London, England)* 360 (9341), 1233–1242.
- Brunekreef, B., Strak, M., Chen, J., Andersen, Z.J., Atkinson, R., Bauwelinck, M., Bellander, T., Boutron, M., Brandt, J., Carey, I., Cesaroni, G., Forastiere, F., Fehst, D., Gulliver, J., Hertel, O., Hoffmann, B., de Hoogh, K., Houthuijs, D., Hvidtfeldt, U., Janssen, N., Jorgensen, J., Katsouyanni, K., Ketzel, M., Klompmaker, J., Hjertager Krog, N., Liu, S., Ljungman, P., Mehta, A., Nagel, G., Oftedal, B., Pershagen, G., Peters, A., Raaschou-Nielsen, O., Renzi, M., Rodopoulou, S., Samoli, E., Schwarze, P., Sigsgaard, T., Stafoggia, M., Vienneau, D., Weinmayr, G., Wolf, K., Hoek, G., 2021. Mortality and Morbidity Effects of Long-Term Exposure to Low-Level PM(2.5), BC, NO(2), and O(3): An Analysis of European Cohorts in the ELAPSE Project. *Research Report (health Effects Institute)* 2021 (208), 1–127.
- Carson, J., Moses, H., 1969. The Validity of Several Plume Rise Formulas. *J. Air Pollut. Control Assoc.* 19 (11), 862–866.
- Jie, C., Sophia, R., de, H. K., Maciej, S., Andersen Zorana J., Richard, A., Mariska, B., Tom, B., Brandt Jørgen, Giulia, C., Hans, C., Daniela, F., Francesco, F., John, G., Ole, H., Barbara, H., Hvidtfeldt, U. A., Janssen Nicole A. H., Jöckel Karl-Heinz, Jørgensen Jeanette, Klea, K., Matthias, K., Klompmaker Jochem O., Anton, L., Karin, L., Shuo, L., Petter, L., MacDonald Conor J., Magnusson Patrik, K.E., Amar, M., Gabriele, N., Bente, O., Pershagen Göran, Annette, P., Raaschou-Nielsen Ole, Matteo, R., Debora, R., Evangelia, S., van der Schouw Yvonne T., Sara, S., Per, S., Torben, S., Sørensen Mette, Massimo, S., Tjønneland Anne, Daniëlle, V., Gudrun, W., Kathrin, W., Bert, B., Gerard, H., 2021. Long-Term Exposure to Fine Particle Elemental Components and Natural and Cause-Specific Mortality—A Pooled Analysis of Eight European Cohorts within the ELAPSE Project. *Environ. Health Perspect.* 129 (4), 047009. <https://ehp.niehs.nih.gov/doi/10.1289/EHP8368>.
- de Hoogh, K., Chen, J., Gulliver, J., Hoffmann, B., Hertel, O., Ketzel, M., Bauwelinck, M., van Donkelaar, A., Hvidtfeldt, U.A., Katsouyanni, K., Klompmaker, J., Martin, R.V., Samoli, E., Schwartz, P.E., Stafoggia, M., Bellander, T., Strak, M., Wolf, K., Vienneau, D., Brunekreef, B., Hoek, G., 2018. Spatial PM(2.5), NO(2), O(3) and BC models for Western Europe - Evaluation of spatiotemporal stability. *Environ. Int.* 120, 81–92.
- Department for Business, Energy & Industrial Strategy (BEIS 2017). NOx speed-related emission function calculation workbook (COPERT version 5.0.1145). National Atmospheric Emission Inventory, UK, Reference ED62553001. URL: <https://naei.energysecurity.gov.uk/data-archive>.
- Department for Transport (DfT), 2009. Road vehicle emission factors: A review of methods for determining hot exhaust emission factors for road vehicles. Transport Research Laboratory, UK. Reference PPR353.
- Dimakopoulou, K., Samoli, E., Analitis, A., Schwartz, J., Beevers, S., Kitwiroon, N., Beddows, A., Barratt, B., Rodopoulou, S., Zafeiratou, S., Gulliver, J., Katsouyanni, K., 2022. Development and Evaluation of Spatio-Temporal Air Pollution Exposure Models and Their Combinations in the Greater London Area, UK. *Int. J. Environ. Res. Public Health* 19 (9), 5401.
- Dominici, F., Schwartz, J., Di, Q., Braun, D., Choirat, C., Zanobetti, A., 2019. (2019) ‘Assessing Adverse Health Effects of Long-Term Exposure to Low Levels of Ambient Air Pollution: Phase 1’. Research Report (health Effects Institute) 200, 1–51.
- Dominski, F.H., Lorenzetti Branco, J.H., Buonanno, G., Stabile, L., Gameiro da Silva, M., Andrade, A., 2021. Effects of air pollution on health: A mapping review of systematic reviews and meta-analyses. *Environ. Res.* 201, 111487.
- Eeftens, M., Beekhuizen, J., Beelen, R., Wang, M., Vermeulen, R., Brunekreef, B., Huss, A., Hoek, G., 2013. Quantifying urban street configuration for improvements in air pollution models. *Atmos. Environ.* 72, 1–9.
- European Commission (EC), 2008. Directive 2008/50/EC of the European Parliament on ambient air quality and cleaner air for Europe.
- Commission, E., 2014. A harmonised definition of cities and rural areas: The new degree of urbanisation. Regional and Urban Policy, Regional Working Paper.
- European Environment Agency (EEA), 1996. Selected nomenclature for air pollution for CORINEAIR 94 inventory (SNAP 94), version 1.1. European Topic Centre on Air Emissions (ETC/AE).
- Gulliver, J., de Hoogh, K., Hansell, A., Vienneau, D., 2013. Development and back-extrapolation of NO<sub>2</sub> land use regression models for historic exposure assessment in Great Britain. *Environ. Sci. Tech.* 47 (14), 7804–7811.
- Hoek, G., Beelen, R., de Hoogh, K., Vienneau, D., Gulliver, J., Fischer, P., Briggs, D., 2008. A review of land-use regression models to assess spatial variation of outdoor air pollution. *Atmos. Environ.* 42 (33), 7561–7578.
- Jephcote, C., Hansell, A.L., Adams, K., Gulliver, J., 2021. Changes in air quality during COVID-19 ‘lockdown’ in the United Kingdom. *Environ. Pollut.* 272 (Published online: 20 November 2020).
- Johnson, W.B., Ludwig, F.L., Dabberdt, W.F., Allen, R.J., 1973. An Urban Diffusion Simulation Model For Carbon Monoxide. *J. Air Pollut. Control Assoc.* 23 (6), 490–498.
- Kerckhoffs, J., Wang, M., Meliefste, K., Malmqvist, E., Fischer, P., Janssen, N., Beelen, R., Hoek, G., 2015. A national fine spatial scale land-use regression model for ozone. *Environ. Res.* 140, 440–448. <https://doi.org/10.1016/j.envres.2015.04.014>.
- Kilbo Edlund, K., Kisiel, M.A., Asker, C., Segersson, D., Bennet, C., Spanne, M., Gustafsson, S., Lindvall, J., Eneroth, K., Tondel, M., Ljungman, P., Stockfelt, L., Pershagen, G., Molnár, P., 2024. High-resolution dispersion modelling of PM2.5, PM10, NOx and NO2 exposure in metropolitan areas in Sweden 2000–2018 – large health gains due to decreased population exposure. *Air Qual. Atmos. Health*. <https://doi.org/10.1007/s11869-024-01535-0>.
- Klompmaker, J.O., Janssen, N., Andersen, Z.J., Atkinson, R., Bauwelinck, M., Chen, J., de Hoogh, K., Houthuijs, D., Katsouyanni, K., Marra, M., Oftedal, B., Rodopoulou, S., Samoli, E., Stafoggia, M., Strak, M., Swart, W., Wesseling, J., Vienneau, D., Brunekreef, B., Hoek, G., 2021. Comparison of associations between mortality and

- air pollution exposure estimated with a hybrid, a land-use regression and a dispersion model. *Environ. Int.* 146, 106306.
- Knibbs, L.D., Hewson, M.G., Bechle, M.J., Marshall, J.D., Barnett, A.G., 2014. A national satellite-based land-use regression model for air pollution exposure assessment in Australia. *Environ. Res.* 135, 204–211.
- Korek, M., Johansson, C., Svensson, N., Lind, T., Beelen, R., Hoek, G., Pershagen, G., Bellander, T., 2017. Can dispersion modeling of air pollution be improved by land-use regression? An example from Stockholm, Sweden. *J. Exposure Sci. Environ. Epidemiol.* 27 (6), 575–581.
- Kučera, T., Chochołač, J., 2021. Design of the City Logistics Simulation Model Using PTV VISSIM Software. *Transp. Res. Procedia* 53, 258–265.
- Lott, N., 2003. The quality control of the integrated surface hourly database. National Oceanic and Atmospheric Administration, National Climatic Data Center, Asheville, North Carolina, USA. URL: [www.nccl.noaa.gov/pub/data/inventories/ish-qc.pdf](http://www.nccl.noaa.gov/pub/data/inventories/ish-qc.pdf).
- Lu, T., Marshall, J.D., Zhang, W., Hystad, P., Kim, S., Bechle, M.J., Demuzere, M., Hankey, S., 2021. National Empirical Models of Air Pollution Using Microscale Measures of the Urban Environment. *Environ. Sci. Tech.* 55 (22), 15519–15530.
- Ma, X., Zou, B., Deng, J., Gao, J., Longley, I., Xiao, S., Guo, B., Wu, Y., Xu, T., Xu, X., Yang, X., Wang, X., Tan, Z., Wang, Y., Morawska, L., Salmond, J., 2024. A comprehensive review of the development of land use regression approaches for modeling spatiotemporal variations of ambient air pollution: A perspective from 2011 to 2023. *Environ. Int.* 183, 108430.
- Madaro, F., Mehdipour, I., Caricato, A., Guido, F., Rizzi, F., Carlucci, A., De Vittorio, M., 2020. Available Energy in Cars' Exhaust System for IoT Remote Exhaust Gas Sensor and Piezoelectric Harvesting. *Energies* 2020 (13), 4169.
- Masey, N., Hamilton, S., Beverland, I.J., 2018. Development and evaluation of the RapidAir® dispersion model, including the use of geospatial surrogates to represent street canyon effects. *Environ. Model. Softw.* 108, 253–263.
- McElroy, J.L., Pooler, F., 1968. The St. Louis Dispersion Study. U.S. Public Health Service, National Air Pollution Control Administration. Report AP-53.
- Mitchell, A.E., 1982. A comparison of short-term dispersion estimates resulting from various atmospheric stability classification methods. *Atmos. Environ.* 16 (4), 765–773.
- Ndiaye, A., Shen, Y., Kyriakou, K., Karssenberg, D., Schmitz, O., Flückiger, B., Hoogh, K., Hoek, G., 2024. Hourly land-use regression modeling for NO<sub>2</sub> and PM<sub>2.5</sub> in the Netherlands. *Environ. Res.* 256, 119233.
- Morley, D., Gulliver, J., 2016. Methods to improve traffic flow and noise exposure estimation on minor roads. *Environ. Pollut.* 216, 746–754.
- National Oceanic and Atmospheric Administration (NOAA), 2018. Federal climate complex data documentation for Integrated Surface Data. Dataset ID: DS3505. Asheville, North Carolina, USA. URL: [www.nccl.noaa.gov/data/global-hourly/doc/isd-format-document.pdf](http://www.nccl.noaa.gov/data/global-hourly/doc/isd-format-document.pdf).
- Naughton, O., et al., 2018. A land use regression model for explaining spatial variation in air pollution levels using a wind sector based approach. <https://doi.org/10.1016/j.scitotenv.2018.02.317>.
- Novotny, E.V., Bechle, M.J., Millet, D.B., Marshall, J.D., 2011. National Satellite-Based Land-Use Regression: NO<sub>2</sub> in the United States. *Environ. Sci. Tech.* 45 (10), 4407–4414.
- Organisation for Economic Co-operation and Development (OECD), 2016. OECD Regional Outlook 2016: Productive Regions for Inclusive Societies. OECD Publishing, Paris.
- Ordnance Survey (OS), 2023. OS MasterMap topography layer™: Technical specification. UK Government, Southampton.
- Pasquill, F., 1961. The estimation of the dispersion of windborne material. *The Meteorology Magazine* 90 (1063), 33–49.
- Perillo, G., Piccolo, M., 1991. An interpolation method for estuarine and oceanographic data. *Comput. Geosci.* 17 (6), 813–820.
- Qi, M., Dixit, K., Marshall, J.D., Zhang, W., Hankey, S., 2022. National Land Use Regression Model for NO<sub>2</sub> Using Street View Imagery and Satellite Observations. *Environ. Sci. Tech.* 56 (18), 13499–13509.
- Shen, Y., de Hoogh, K., Schmitz, O., Gulliver, J., Vienneau, D., Vermeulen, R., Hoek, G., Karssenberg, D., 2024. Europe-wide high-spatial resolution air pollution models are improved by including traffic flow estimates on all roads. *Atmos. Environ.* 335, 120719.
- Sfyridis, A., Agnolucci, P., 2023. Factors Affecting Road Traffic: Identifying Drivers of Annual Average Daily Traffic Using Least Absolute Shrinkage and Selection Operator Regression. *Transp. Res. Rec.* 2677 (5), 1178–1192.
- Stevens, F.R., Gaughan, A.E., Linard, C., Tatem, A.J., 2015. Disaggregating Census Data for Population Mapping Using Random Forests with Remotely-Sensed and Ancillary Data. *PLoS One* 10.
- Stineman, R., 1980. A consistently well-behaved method of interpolation. *Creative Computing* 6 (7), 54–57.
- Stull, R., 1988. An introduction to boundary layer meteorology. Kluwer Academic Publishers, The Netherlands.
- Tang, D., Zhan, Y., Yang, F., 2024. A review of machine learning for modeling air quality: Overlooked but important issues. *Atmos. Res.* 300, 107261.
- Townsend, P., Phillimore, P., Beattie, A., 1989. *Health and Deprivation Inequality and the North*. Routledge, London, UK. <https://doi.org/10.4324/9781003368885>.
- Tukey, J., 1977. *Exploratory data analysis*. Addison-Wesley, Reading, Massachusetts, USA.
- Tularam, H., Ramsay, L.F., Muttoo, S., Brunekreef, B., Meliefste, K., de Hoogh, K., Naidoo, R.N., 1987. (2021) 'A hybrid air pollution / land use regression model for predicting air pollution concentrations in Durban, South Africa', *Environmental Pollution* (Barking. Essex 274, 116513.
- Turner, D.B., 1964. A diffusion model for an urban area. *J. Appl. Meteorol. Climatol.* 3 (1), 83–91.
- Turner, B., 1970. Workbook of atmospheric dispersion estimates. US Department of health, education, and welfare. Public Health Service Publication No, Cincinnati, Ohio, USA.
- U.S. Environmental Protection Agency (USEPA), 1995. User's Guide for the Industrial Source Complex (ISC3) Dispersion Models, Volume 2: Description of Model Algorithms. No. 4541B-95-003B. Office of Air Quality Planning and Standards, North Carolina.
- U.S. Environmental Protection Agency (USEPA), 2000. Meteorological Monitoring Guidance for Regulatory Modeling Applications. No. EPA-454/R-99-005. Office of Air Quality Planning and Standards, North Carolina.
- US Nuclear Regulatory Commission (USNRC), 1972. Meteorological Programs in Support of Nuclear Power Plants. Regulatory Guide 1.23. U.S. Nuclear Regulatory Commission, Office of Standards Development, Washington, DC (Docket No. A-80-46, II-P-11).
- Vachon, J., Kerckhoffs, J., Buteau, S., Smargiassi, A., 2024. 'Do machine learning methods improve prediction of ambient air pollutants with high spatial contrast? A Systematic Review', *Environmental Research* 262, 119751.
- Vardoulakis, S., Fisher, B., Gonzalez-Flesca, N., Pericleous, K., 2002. Estimates of Uncertainty in Urban Air Quality Model Predictions. In: Borrego, C., Schayes, G. (eds.), *Air Pollution Modeling and Its Application XV*. Boston, MA: Springer US, pp. 483–491. [https://doi.org/10.1007/0-306-47813-7\\_49](https://doi.org/10.1007/0-306-47813-7_49).
- Wang, W., Fecht, D., Beevers, S., Gulliver, J., 2022. Predicting daily concentrations of nitrogen dioxide, particulate matter, and ozone at fine spatial scale in Great Britain. *Atmos. Pollut. Res.* 13(8), 101506. Retrieved from Atmospheric Pollution Research. <https://doi.org/10.1016/j.apr.2022.101506>.
- World Health Organization (WHO), 2021. WHO global air quality guidelines: particulate matter (PM<sub>2.5</sub> and PM<sub>10</sub>), ozone, nitrogen dioxide, sulfur dioxide and carbon monoxide. ISBN 9789240034228.
- Whittaker, J., Whitehead, C., Mark, S., 2005. The Neglog Transformation and Quantile Regression for the Analysis of a Large Credit Scoring Database. *J. Roy. Stat. Soc.: Ser. C (Appl. Stat.)* 54 (5), 863–878.
- Xu, H., Bechle, M.J., Wang, M., Szpiro, A.A., Vedal, S., Bai, Y., Marshall, J.D., 2019. National PM<sub>2.5</sub> and NO<sub>2</sub> exposure models for China based on land use regression, satellite measurements, and universal kriging. *Sci. Total Environ.* 655, 423–433.
- Yamartino, R.J., 1984. A Comparison of Several "Single-pass" Estimators of the Standard Deviation of Wind Direction. *J. Climate Appl. Meteor.* 23, 1362–1366.
- Zhou, Y., et al., 2010. Accounting for surface reflectance anisotropy in satellite retrievals of tropospheric NO<sub>2</sub>. *Atmos. Meas. Tech.* 3, 1185–1203. <https://doi.org/10.5194/amt-3-1185-2010>. <https://amt.copernicus.org/articles/3/1185/2010/>.